Palaeomagnetic study of a sub-aerial volcanic ridge (Sao Jorge Island, Azores) for the past 1.3 Myr : evidence for the Cobb Mountain Subchron, volcano flank instability and tectono-magmatic implications

P.F. Silva, B. Henry, F.O. Marques, A. Hildenbrand, P. Madureira, C.A. Mériaux, Z. Kratinova

Geophysical Journal International

Geophys. J. Int. (2012) **188,** 959–978 doi: 10.1111/j.1365-246X.2011.05320.x

Palaeomagnetic study of a subaerial volcanic ridge (São Jorge Island, Azores) for the past 1.3 Myr: evidence for the Cobb Mountain Subchron, volcano flank instability and tectonomagmatic implications

P. F. Silva,[1] B. Henry,[2] F. O. Marques,[3] A. Hildenbrand,[4,5] P. Madureira,[6] C. A. Mériaux[3] and Z. Kratinová[3,7]

[1]*ISEL/DEC and IDL (Universidade de Lisboa), Lisboa, Portugal. E-mail: pmfsilva@fc.ul.pt*
[2]*Palaeomagnetism, IPGP and CNRS, Saint-Maur cedex, France*
[3]*Universidade de Lisboa, IDL, Lisboa, Portugal*
[4]*Université Paris-Sud, Laboratoire IDES, UMR8148, Orsay,* F-91405, *France*
[5]*CNRS, Orsay,* F-91405, *France*
[6]*Centro de Geofísica de Évora and Departamento de Geociências, Universidade de Évora, Évora, Portugal*
[7]*Institute of Geophysics, Academy of Sciences of the Czech Republic, Prague, Czech Republic*

Accepted 2011 November 28. Received 2011 November 17; in original form 2011 September 3

SUMMARY

We present a palaeomagnetic study on 38 lava flows and 20 dykes encompassing the past 1.3 Myr on S. Jorge Island (Azores Archipelago—North Atlantic Ocean). The sections sampled in the southeastern and central/western parts of the island record reversed and normal polarities, respectively. They indicate a mean palaeomagnetic pole (81.3°N, 160.7°E, $K = 33$ and $A_{95} = 3.4°$) with a latitude shallower than that expected from Geocentric Axial Dipole assumption, suggesting an effect of non-dipolar components of the Earth magnetic field. Virtual Geomagnetic Poles of eight flows and two dykes closely follow the contemporaneous records of the Cobb Mountain Subchron (ODP/DSDP programs) and constrain the age transition from reversed to normal polarity at *ca.* 1.207 ± 0.017 Ma. Volcano flank instabilities, probably related to dyke emplacement along an NNW–SSE direction, led to southwestward tilting of the lava pile towards the sea. Two spatially and temporally distinct dyke systems have been recognized on the island. The eastern is dominated by NNW–SSE trending dykes emplaced before the end of the Matuyama Chron, whereas in the central/western parts the eruptive fissures oriented WNW–ESE controlled the westward growth of the S. Jorge Island during the Brunhes Chron. Both directions are consistent with the present-day regional stress conditions deduced from plate kinematics and tectonomorphology and suggest the emplacement of dykes along pre-existing fractures. The distinct timing and location of each dyke system likely results from a slight shift of the magmatic source.

Key words: Palaeomagnetic secular variation; Palaeomagnetism applied to tectonics; Palaeomagnetism applied to geologic processes; Reversals: process, time scale, magnetostratigraphy; Rock and mineral magnetism; Atlantic Ocean.

1 INTRODUCTION

Palaeomagnetism is the only tool that enables the study of the ancient geomagnetic field behaviour. To improve the quality of global geomagnetic field models, it is necessary to improve the spatial–temporal coverage. The nine islands of the Azores Archipelago in the North Atlantic are preferential targets for such propose, because they comprise a large amount of thick lava piles, some of which have been isotopically dated. However, to our knowledge only one palaeomagnetic study has been reported for S. Miguel Island in the Azores (Johnson *et al.* 1998).

The island of S. Jorge is a volcanic ridge, elongated along the WNW–ESE direction (Fig. 1a). Recently, new precise geochronological data on lava successions exposed along the island width have evidenced distinct and fast phases of volcanic construction since *ca.* 1.3 Ma (Hildenbrand *et al.* 2008). Dyke swarms with three main orientations intruded the various lava piles, but are still of unknown absolute age.

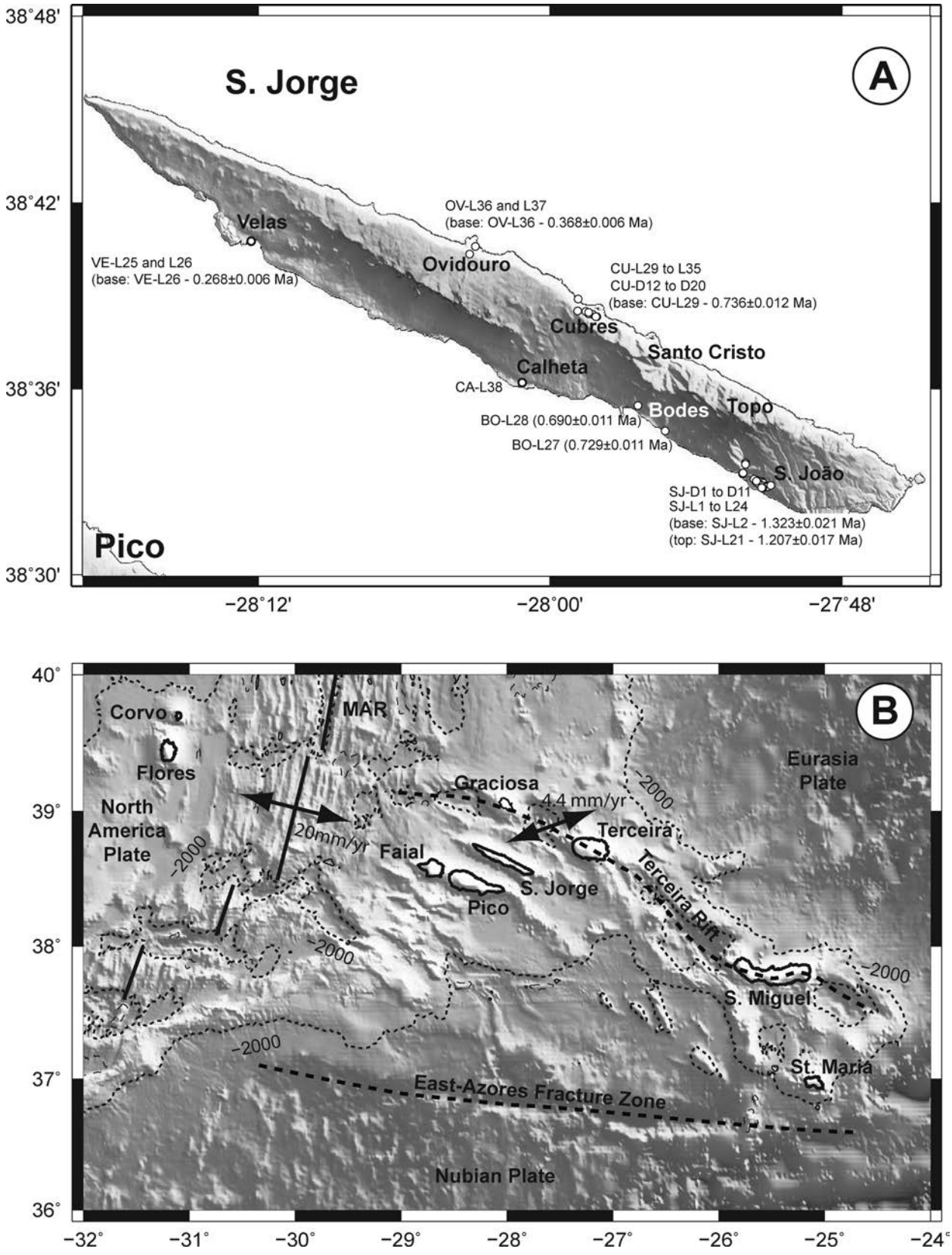

Figure 1. (a) Topographic map of S. Jorge Island with indication of sampling sites and respective ages obtained by Hildenbrand *et al.* (2008). (b) Shaded relief of the Azores Plateau with indication of the islands and main morphotectonic structures; MAR, Mid-Atlantic Ridge.

Given the importance of a better understanding of the Pleistocene Earth's magnetic field, a palaeomagnetic study on S. Jorge represents an excellent opportunity to obtain reliable palaeomagnetic data for secular variation and magnetostratigraphy studies of the last 1.3 Myr. Furthermore, it represents an excellent opportunity to investigate the intrusive history of this island, which could also contribute to the knowledge of the tectonic setting responsible for the construction/destruction of the Azores islands.

To obtain the new palaeomagnetic data, we have chosen to study six different sections that include eight lava flows previously dated by K/Ar (Hildenbrand *et al.* 2008) and two newly dated lava flows (Tables 1 and 2). The new geochronological analyses have been acquired on fresh-separated groundmass, following the same protocol of sample preparation and analytical procedure than the one described in Hildenbrand *et al.* (2008). The analyses have been carried out with the unspiked K/Ar Cassignol–Gillot technique (Cassignol & Gillot 1982), which has been shown especially suitable to date precisely young basaltic lava flows (e.g. Hildenbrand *et al.* 2004; Gillot *et al.* 2006; Boulesteix *et al.* 2012). Dykes were also sampled in two of these sections.

2 GEOLOGICAL SETTING

2.1 The Azores Plateau

The Azores Archipelago is located in the North Atlantic Ocean and includes nine volcanic islands, which developed on the eastern and western flanks of the Mid-Atlantic Ridge (MAR). These islands sit on top of a bathymetric anomaly confined by the 2000 m isobath, which delineates a triangular shaped area known as the Azores Plateau (see Fig. 1b). This plateau records tectonic and volcanic morphologies that result from complex interactions between the Azores Triple Junction and the Azores hotspot (e.g. Searle 1980; Madeira & Ribeiro 1990; Luis *et al.* 1994; Lourenço *et al.* 1998; Miranda *et al.* 1998; Cannat *et al.* 1999; Gente *et al.* 2003; Madureira *et al.* 2005, 2011; Lourenço 2007; Luis & Miranda 2008), combined with the hyperslow spreading rate at the Terceira Rift (Vogt & Jung 2004).

Aeromagnetic and bathymetric data show that the islands of the central group represent high and WNW–ESE aligned positive magnetic anomalies, interpreted as neovolcanic axes that define linear volcanic ridges (LVR; Miranda *et al.* 1991; Luis *et al.* 1994). The morphology of the Azores Plateau points to the presence of two distinct sets of LVRs (Lourenço *et al.* 1998), which are aligned along the WNW–ESE (N110°–N120°) and NNW–SSE (N140°–N150°) directions. According to Madeira & Ribeiro (1990), Lourenço *et al.* (1998) and Miranda *et al.* (1998), these LVRs are the morphological expressions of the tectonic setting driven by a right-lateral transtensional regime related to the eastward movement of Eurasia relative to a fixed Africa (DeMets *et al.* 1994). Vogt & Jung (2004) and Lourenço (2007) attributed the two LVR directions to changes of the stress field and promoted by the interaction between the Azores hotspot and the Azores Triple Junction migrations. Geochronological data for the Faial–Pico Ridge (Beier 2006) and for the S. Jorge ridge (Hildenbrand *et al.* 2008) show a distinct time of emplacement of the flows of the two systems of LVRs, the flows of the WNW–ESE system being the youngest.

2.2 S. Jorge Island

S. Jorge is a volcanic ridge elongated along the WNW–ESE azimuth (55 km long per 7 km of maximum width—Fig. 1a). Morphologically, the island is characterized by high coastal cliffs, that can reach 500 m above sea level (see Figs 2a and b). The cliffs are particularly steep along the northern coast, which is more exposed to erosional agents. Most villages are located on lava fans locally called 'Fajãs' (e.g. Ovidouro, Velas and Calheta in Fig. 1a) or on mass wasted deposits due to sea-cliff gravitational instability (e.g. S. João, Cubres and Santo Cristo in Fig. 1a).

Geochronological data revealed an emerged build-up of the island that started at least 1.3 Ma (Hildenbrand *et al.* 2008). According to these authors, the early development of the island first involved the construction of an NNW–SSE ridge between 1.3 and 1.2 Ma. After an apparent gap of *ca.* 450 kyr, the subsequent main volcanic activity migrated to the West, and was responsible for the construction of the central-western domains of the island during the last 750 kyr. The various volcanic successions of S. Jorge are cut by numerous dykes with individual thickness ranging between 1 and 3 m. They are mostly vertical and show distinct orientations according to the geographical sectors of the island. Dykes are abundant and preferentially aligned along the NNW–SSE direction in the eastern part, and trend along the WNW–ESE in the central-western domain (Fig. 2e). Some dykes were also observed along the N60° azimuth. On the eastern part of the island (Fajã de S. João), evidence of dip-slip movement along dyke walls and fault planes have been observed in this study (Figs 2c and d), as already described by Madeira (1998).

3 SAMPLING AND METHODS

To accomplish our objectives, 38 lava flows and 20 dykes were sampled for palaeomagnetism and rock magnetism studies (Fig. 1b): 24 flows (259 samples) and 11 dykes (87 samples) at S. João (SJ); two flows (24 samples) at Bodes (BO); one flow (eight samples) at Calheta (CA); two flows (23 samples) at Velas (VE); seven flows (65 samples) and nine dykes (66 samples) at Cubres, Fajã da Ponta (CU) and two flows (19 samples) at Ovidouro (OV).

We used a CS3 furnace coupled to a KLY3 Kappabridge to determine the main carriers of remanent magnetization by means of thermomagnetic and high-field experiments. Analyses of low-field magnetic susceptibility as a function of temperature, $K(T)$, were performed until a maximum temperature of 600–700°C, under an argon controlled atmosphere.

To infer the petrofabric and possible effects of the ferromagnetic grains anisotropy on the palaeomagnetic directions, the anisotropy of magnetic susceptibility (AMS) was measured with KLY3 and MFK1-FA Kappabridges. The shape of the magnetic ellipsoid was characterized using Jelinek (1981) parameters (corrected degree of anisotropy, P', and shape parameter, T). The orientation of the magnetic ellipsoid was determined by tensor variability statistics (Hext 1963; Jelinek 1978).

Classical determinations of hysteresis loops were carried out with a laboratory-made translation inductometer within an electromagnet. These experiments were complemented by the study of isothermal remanent magnetization (IRM) acquisition using an impulse magnetizer IM-10–30 and a JR-6 magnetometer. IRM data underwent cumulative log-Gaussian analyses (Robertson & France 1994; Kruiver *et al.* 2001). Complementarily, we conducted a detailed microscopic observation of the magnetic carriers from representative samples from the Fajã de S. João as well as from the Fajã dos Cubres. It was performed on a JEOL JSM-6400 Scanning Electron Microscope (SEM) coupled with an OXFORD Energy Dispersive Spectrometer (EDS) Si(Li) X-ray detector housed at Centro Hércules,

Table 1. Palaeomagnetic results obtained for S. Jorge Island: Long. and Lat., geographic longitude and latitude of sampling site; N_d/N , number of demagnetized samples/number of samples used for site mean ChRM; D and I, mean declination and inclination of the mean ChRM; k and K, precision parameters; α_{95} and A_{95}, 95 per cent confidence limit of the mean directions (Fisher 1953); VGP Long (°) and VGP Lat (°), longitude and latitude of the VGP (and of the palaeomagnetic pole for the mean direction). Mean direction calculated for a cut-off angle of 45°; ∗, K/Ar ages from Hildenbrand *et al.* (2008); ∗∗, new K/Ar ages measured in this study (see Table 2); dykes (∗∗∗, dykes at Cubres with N60° azimuth). Correspondence between the nomenclature of lava flows used by this study and the work of Hildenbrand *et al.* (2008), the latter between parenthesis: SJ-L2 (AZ05-P); SJ-L5 (AZ05-AR); SJ-L9 (AZ05-U); SJ-L15 (AZ05-Z); SJ-L21 (AZ05-AB); VE-L26 (AZ05-AJ); BO-L27 (AZ05-AF); BO-L28 (AZ05-AG); CU-L29 (AZ05-AD); OV-L36 (AZ05-AH).

Site	Long. (°)	Lat. (°)	N_d/N	D (°)	I (°)	k	α_{95} (°)	VGP Long. (°)	VGP Lat. (°)	K	A_{95} (°)	Age (Ma)
Reverse polarity—Eastern domain (Fajã of S. João)												
Lava flows												
SJ-L1	−27.866	38.560	12/11	199.4	−29.1	100	4.2	14.2	−61.5	117	3.9	
SJ-L2	−27.866	38.560	12/10	164.9	−45.8	270	2.7	25.2	−73.1	254	2.8	1.323 ± 0.021*
SJ-L3	−27.866	38.559	12/12	173.9	−45.8	189	2.9	−2.1	−77.7	166	3.1	
SJ-L4	−27.855	38.547	10/9	187.4	−43.7	83	5.1	−55.3	−75.3	59	5.8	
SJ-L5	−27.855	38.547	12/12	183.3	−41.7	198	2.9	−39.9	−75.3	203	2.8	1.310 ± 0.019*
SJ-L6	−27.855	38.547	11/9	178.2	−47.9	175	3.5	−17.6	−80.5	187	3.4	
SJ-L7	−27.855	38.547	13/13	179.7	−32.0	130	3.4	−26.7	−68.9	139	3.3	
SJ-L8	−27.855	38.548	13/12	192.9	−26.7	94	4.2	−60.1	−62.0	63	4.9	
SJ-L9	−27.855	38.548	12/9	216.5	−6.9	122	4.2	−80.6	−41.7	160	3.7	1.314 ± 0.019**
SJ-L10	−27.855	38.548	12/12	178.4	−32.3	210	2.8	−23.7	−69.0	268	2.5	
SJ-L11	−27.859	38.551	10/10	195.8	−51.2	337	2.4	−95.7	−75.6	288	2.6	
SJ-L12	−27.858	38.550	12/12	181.4	−33.3	164	3.3	−31.5	−69.7	164	3.2	
SJ-L13	−27.858	38.550	12/12	173.3	−40.6	133	3.5	−5.2	−73.8	163	3.2	
SJ-L14	−27.858	38.550	13/13	181.7	−22.7	202	2.7	−31.4	−63.3	272	2.4	
SJ-L15	−27.857	38.550	13/13	198.1	−57.1	96	4.0	−121.6	−75.4	58	5.1	1.267 ± 0.018**
SJ-L16	−27.856	38.550	11/11	183.5	−20.8	300	2.4	−35.1	−62.1	421	2.1	
SJ-L17	−27.855	38.550	13/11	193.4	−41.6	127	3.7	−67.2	−69.8	106	3.8	
SJ-L18	−27.854	38.550	15/15	209.0	−20.3	41	5.7	−78.6	−51.8	44	5.4	
SJ-L19	−27.855	38.549	9/9	219.7	−22.1	491	2.1	−91.2	−45.5	540	2.0	
SJ-L20	−27.854	38.549	9/7	196.4	−30.9	356	2.8	−65.7	−63.8	453	2.5	
SJ-L21	−27.851	38.548	13/10	328.4	−40.1	41	6.9	−176.4	21.5	35	7.5	1.207 ± 0.017*
SJ-L22	−27.851	38.548	11/9	304.6	−42.5	71	5.6	−158.7	7.9	63	5.9	
SJ-L23	−27.851	38.547	9/9	184.4	−36.3	258	2.9	−40.7	−71.3	228	3.1	
SJ-L24	−27.848	38.548	9/9	235.6	2.3	191	3.4	−93.8	−25.5	232	3.1	
Dykes												
SJ-D1	−27.868	38.554	8/7	175.2	−48.1	217	4.1	−3.7	−79.9	168	4.7	
SJ-D2	−27.868	38.554	6/6	189.6	−60.3	414	3.3	−140.8	−82.2	284	4.0	
SJ-D3	−27.855	38.547	8/7	173.5	−40.1	451	2.8	−6.7	−73.4	441	2.9	
SJ-D4	−27.855	38.547	10/8	236.7	−55.3	345	3.0	−132.8	−45.5	193	4.0	
SJ-D5	−27.854	38.546	8/7	172.8	−46.0	975	1.9	2.8	−77.3	688	2.3	
SJ-D6	−27.856	38.548	10/10	237.7	−62.5	91	5.1	−144.9	−47.4	45	7.3	
SJ-D7	−27.857	38.549	9/9	181.6	−44.1	470	2.4	−34.8	−77.3	345	2.8	
SJ-D8	−27.859	38.550	9/9	182.1	−51.2	618	2.1	−42.2	−83.7	424	2.5	
SJ-D9	−27.860	38.551	8/8	173.4	−37.0	337	3.0	−8.1	−71.3	395	2.8	
SJ-D10	−27.855	38.546	8/6	188.9	−43.6	249	4.3	−60.4	−75.0	228	4.4	
SJ-D11	−27.858	38.550	8/8	179.1	−47.0	287	3.3	−23.3	−79.6	188	4.0	
Mean			**32**	**188.9**	**−40.7**	**21**	**5.7**					
Mean (after rotation of SJ-L1 to L24)			**30**	**179.1**	**−46.5**	**31**	**4.8**					
Normal polarity—Central and Western domains												
Lava flows												
VE-L25	−28.204	38.679	11/11	358.1	48.6	149	3.5	162.0	81.0	138	3.6	
VE-L26	−28.204	38.679	12/12	13.5	44.0	248	2.6	106.4	73.4	262	2.6	0.268 ± 0.006*
BO-L27	−27.921	38.577	12/12	27.0	50.4	281	2.4	72.3	66.9	278	2.4	0.729 ± 0.011*
BO-L28	−27.939	38.590	12/12	358.6	38.4	91	4.2	156.3	73.2	95	4.2	0.690 ± 0.011*
CU-L29	−27.968	38.638	11/11	354.0	58.4	134	3.6	−106.3	85.6	79	4.8	0.736 ± 0.012*
CU-L30	−27.968	38.638	8/8	357.1	38.3	116	4.6	178.9	77.0	123	4.5	
CU-L31	−27.968	38.638	9/9	353.5	55.2	416	2.3	−145.1	84.2	270	2.8	
CU-L32	−27.971	38.639	8/8	345.9	55.6	201	3.5	−125.7	78.7	117	4.6	
CU-L33	−27.974	38.640	12/12	5.2	54.1	211	2.8	102.3	84.3	153	3.3	
CU-L34	−27.973	38.641	9/9	359.9	57.3	335	2.6	155.6	89.4	202	3.3	
CU-L35	−27.980	38.648	8/8	5.1	55.5	167	3.8	90.5	85.2	122	4.5	
OV-L36	−28.055	38.672	11/10	340.9	62.8	73	5.2	−89.2	74.8	34	7.5	0.368 ± 0.006*
OV-L37	−28.051	38.676	9/9	19.7	59.4	368	2.4	49.3	74.7	241	3.0	
CA-L38	−28.019	38.603	8/8	359.0	58.8	539	2.1	−63.7	88.7	369	2.6	

Table 1. (*Continued.*)

Site	Long. (°)	Lat. (°)	N_d/N	D (°)	I (°)	k	α_{95} (°)	VGP Long. (°)	VGP Lat. (°)	K	A_{95} (°)	Age (Ma)
Dykes												
CU-D12	−27.968	38.638	6/6	353.0	53.1	757	2.4	−157.4	82.5	517	3.0	
CU-D13***	−27.973	38.640	8/8	340.1	48.1	660	2.2	−141.8	71.0	736	2.0	
CU-D14	−27.975	38.641	4/4	346.2	50.4	218	6.2	−146.7	76.6	232	6.0	
CU-D15	−27.981	38.641	8/8	354.8	59.0	478	2.5	−98.8	85.8	314	3.1	
CU-D16	−27.973	38.641	8/8	347.9	51.4	341	3.0	−147.5	78.2	359	2.9	
CU-D17***	−27.973	38.641	8/8	347.7	45.7	434	2.7	−162.4	74.7	479	2.7	
CU-D18	−27.973	38.641	9/8	356.8	46.9	298	3.2	167.0	79.3	301	3.2	
CU-D19***	−27.980	38.648	8/8	10.9	43.1	162	4.4	114.6	73.7	125	5.0	
CU-D20	−27.980	38.648	9/8	348.2	55.4	395	2.8	−130.5	80.2	312	3.1	
Mean			**23**	**357.7**	**52.3**	**67**	**3.7**					
Mean (all data after rotation of SJ-L1 to L24)			**53**	**358.5**	**49.0**	**39**	**3.2**	**160.7**	**81.3**	**33**	**3.4**	

Table 2. New age determinations acquired on well-preserved groundmass with the unspiked K/Ar Cassignol–Gillot technique. The decay constants used are from Steiger & Jäger (1977). The uncertainties are reported at the 1σ level.

Sample	K (per cent)	$^{40}Ar^*$ (per cent)	$^{40}Ar^*$ (10^{12} at/g)	Age (Ma)	Uncertain (Ma)
SJ-L9	1.305	21.5	1.7829	1.308	0.019
		33.0	1.7978	1.319	0.019
			mean	**1.314**	**0.019**
SJ-L15	2.036	51.3	2.7307	1.284	0.018
		52.0	2.6604	1.251	0.018
			mean	**1.267**	**0.018**

Évora University, Portugal. The SEM operated under high vacuum conditions (20.0 kV) and using a beam of 65 keV.

Before demagnetization, the samples were maintained in a zero magnetic field shield for at least 1 month to reduce a possible viscous magnetization. 550 samples were demagnetized for palaeomagnetic studies. The magnetization was measured with JR-5 and JR-6A magnetometers (AGICO, Brno). Demagnetizations by alternating field (AF) and thermal methods underwent 10–14 steps to define the remanent magnetization components with the maximum of reliable points. When the study of pilot samples revealed a complete demagnetization by AF with directional palaeomagnetic data similar to those observed by thermal demagnetization, the AF treatment was preferred. Otherwise, thermal demagnetization was applied.

Principal components analysis (Kirschvink 1980) was used to determine the palaeomagnetic directions (defined by the declination D and the inclination I). Determination of the mean site characteristic remanent magnetization (ChRM) direction and of its associated precision parameter (k) and radius of the angular confidence zone at 95 per cent (α_{95}) was made using Fisher (1953) statistics.

4 MICROSCOPIC ANALYSES

Petrographic analyses were carried out on samples collected in lava flows and dykes (*cf.* Fig. 3). As pointed out by Hildenbrand *et al.* (2008), some of the lava flows show a porphyritic texture, with plagioclase, olivine and clinopyroxene as the main phenocrysts. The fine-grained groundmass is mostly characterized by the presence of plagioclase and oxides with minor olivine and clinopyroxene in the most mafic lavas.

Most of the dyke samples display a subaphyric texture with microlites of plagioclase ± (Ti)magnetite ± ilmenite ± olivine ± clinopyroxene. EDS allowed to semi-quantitatively analyse the composition of the magnetic phases and confirms the observations using optical microscopy. Generally, grains of Ti-magnetite tend to be more abundant and to present more euhedric shapes than ilmenite. The latter can also present a high aspect ratio, which was not observed in Ti-magnetite. Ilmenite laths can also occur within (Ti)magnetite grains. In most studied samples, there is no evidence for low-temperature oxidation of primary (Ti)magnetite crystals with further occurrence of maghemite. Sporadically, the exception relative to the absence of alteration features can be found in the highly porphyritic lava samples from the Fajã dos Cubres, where incipient fringes of maghemite were observed around (Ti)magnetite grains.

5 ROCK MAGNETISM

5.1 Thermomagnetic measurements

Thermomagnetic curves show three distinct shapes according to the relative proportions of the inferred main magnetic phases in lava flows and dykes. The two simplest kinds of curves show reversibility with a unique drop of $K(T)$ values, mostly observed for temperatures above 500°C. For a minority of curves, the drop appears as soon as the heating run starts (Figs 4a and b). Such $K(T)$ drops define a bimodal distribution of Curie temperatures (T_c), between 50–120°C and 500–580°C (Chevallier & Pierre 1932; Petrovský & Kapička 2006). According to O'Reilly (1984) and Dunlop & Özdemir (1997), these two ranges of T_c indicate the presence of titanomagnetite [Fe_{3-x} Ti_x O_4] as the main magnetic carrier, with two distinct molar proportions of Ti^{4+} (defined by the composition parameter x). Following Lattard *et al.* (2006), the first susceptibility drop corresponds to x values around 0.6–0.7 (here called TM60), and the final drop corresponds to x values close to 0–0.1 (magnetite—TM0).

A third kind of $K(T)$ cycles shows two drops: the first one occurs at temperatures above 50–120°C after a hump of $K(T)$ values due to a Hopkinson effect; the second drop occurs at temperatures above 400–500°C. This probably indicates a mixture of TM60 and TM0. Part of the samples with this thermomagnetic behaviour shows irreversible curves (see example in Fig. 4a), pointing to the occurrence of mineral alterations. Partial thermomagnetic cycles reveal irreversibility for a hump of $K(T)$ values between 350 and 450°C. This suggests the inversion of oxidized titanomagnetite, e.g. to titanomaghemite (e.g. Dunlop & Özdemir 1997; Miranda *et al.* 2002).

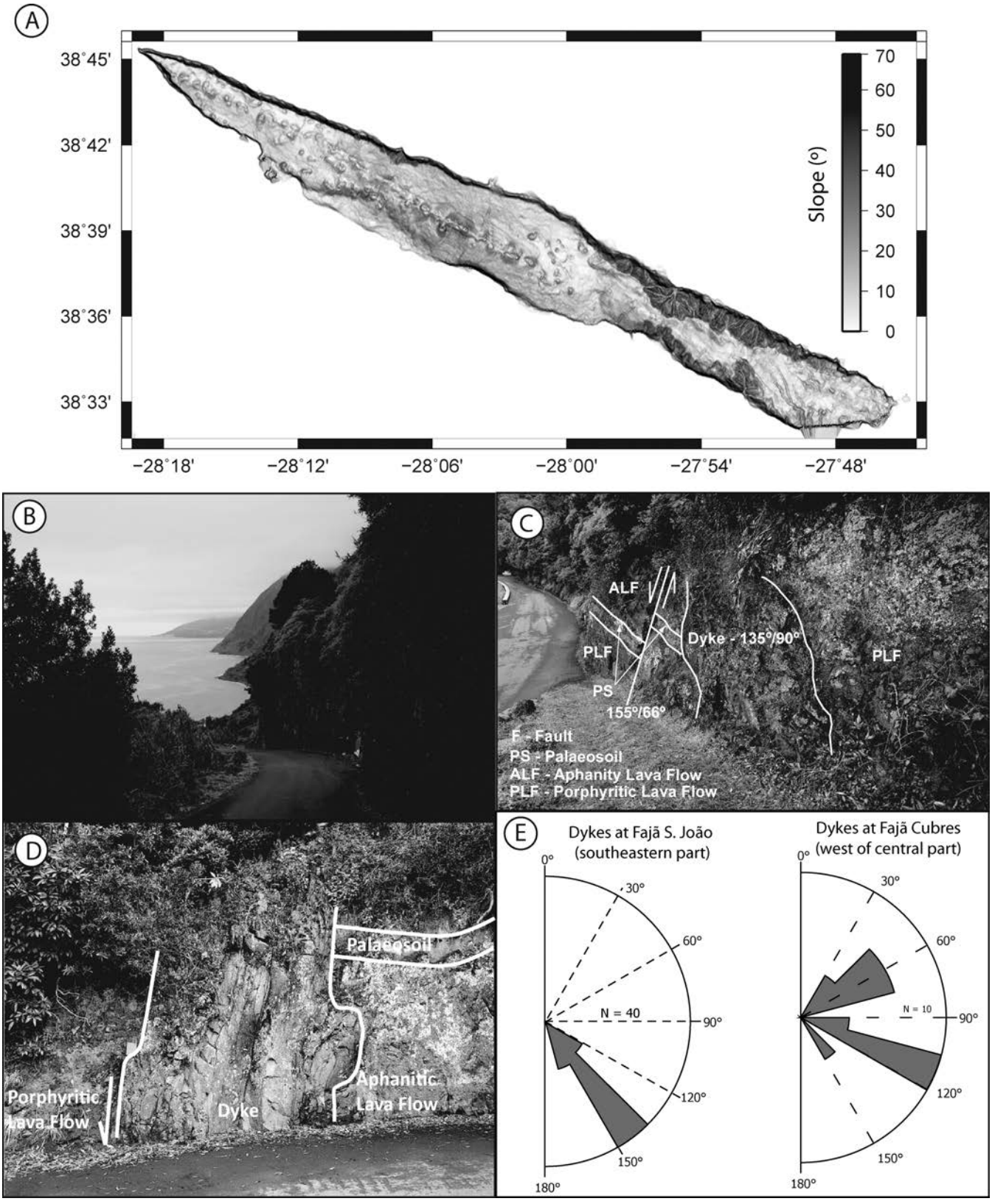

Figure 2. (a) Map with slope inclination (in degrees) of the S. Jorge Island. Image analysis made with the Mirone suite (Luis 2007). (b) Picture representative of the S. Jorge sea cliffs. (c and d) Pictures of S. João sea cliff showing dip-slip movement along dykes and fault planes. (e) Rose diagrams showing the preferential orientation of dyke swarms observed at S. João (eastern domain) and Cubres (central domain, northern margin).

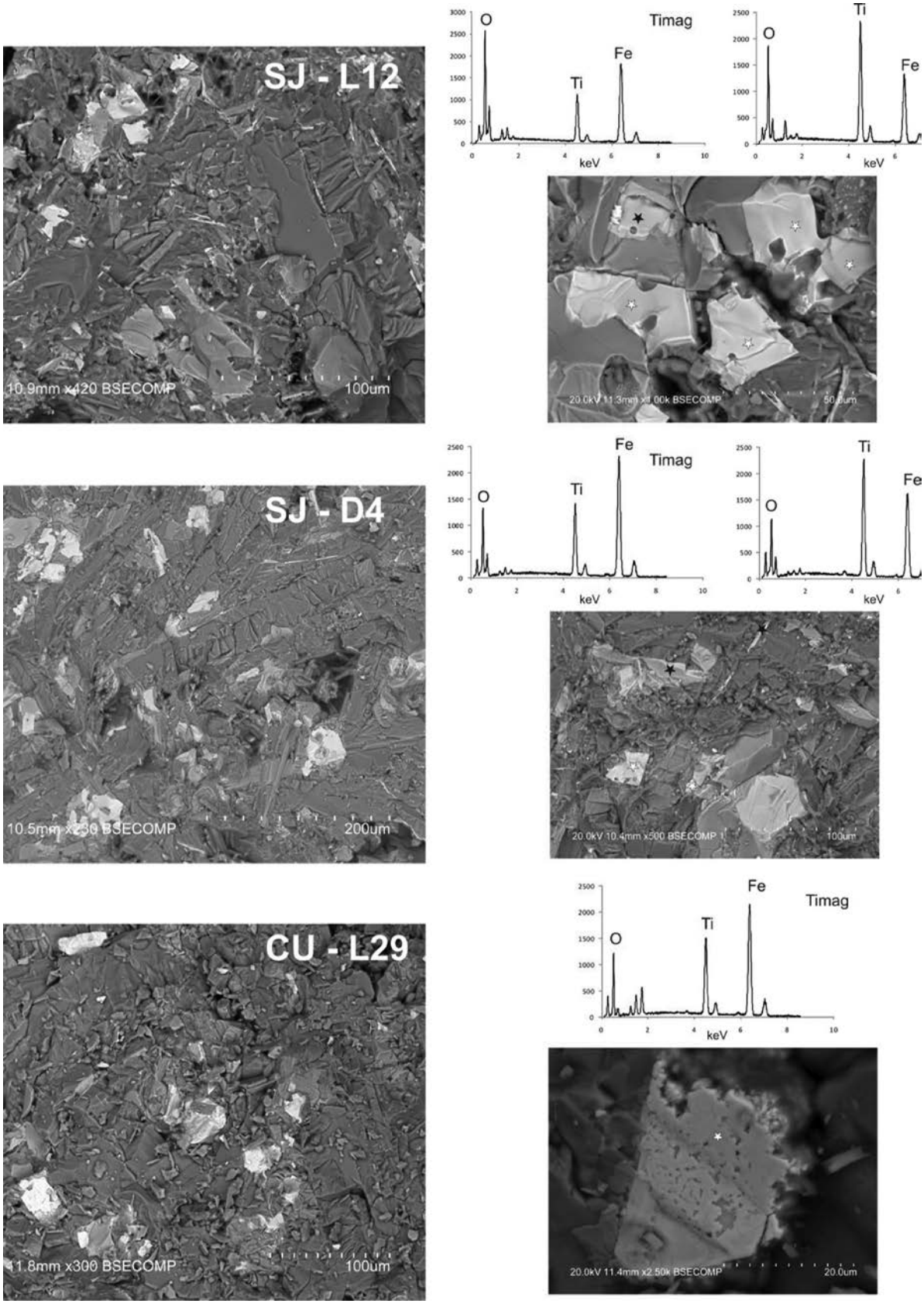

Figure 3. Microscopic textures of selected samples (two lavas, SJ-L12, CU-L29 and one dyke, SJ-D4) studied by SEM (images obtained with secondary electrons). The photos on the left-hand side correspond to general views showing the average proportion and distribution of the main magnetic carriers (i.e. Titanomagnetite and Ilmenite, lighter grains). The photos on the right-hand side are from selected areas for analysis of the magnetic phases. The diagrams shown on top are typical spectra obtained for Titanomagnetite (Timag) and Ilmenite (Ilm). White and black stars in the photos represent analyses on Titanomagnetite and Ilmenite, respectively.

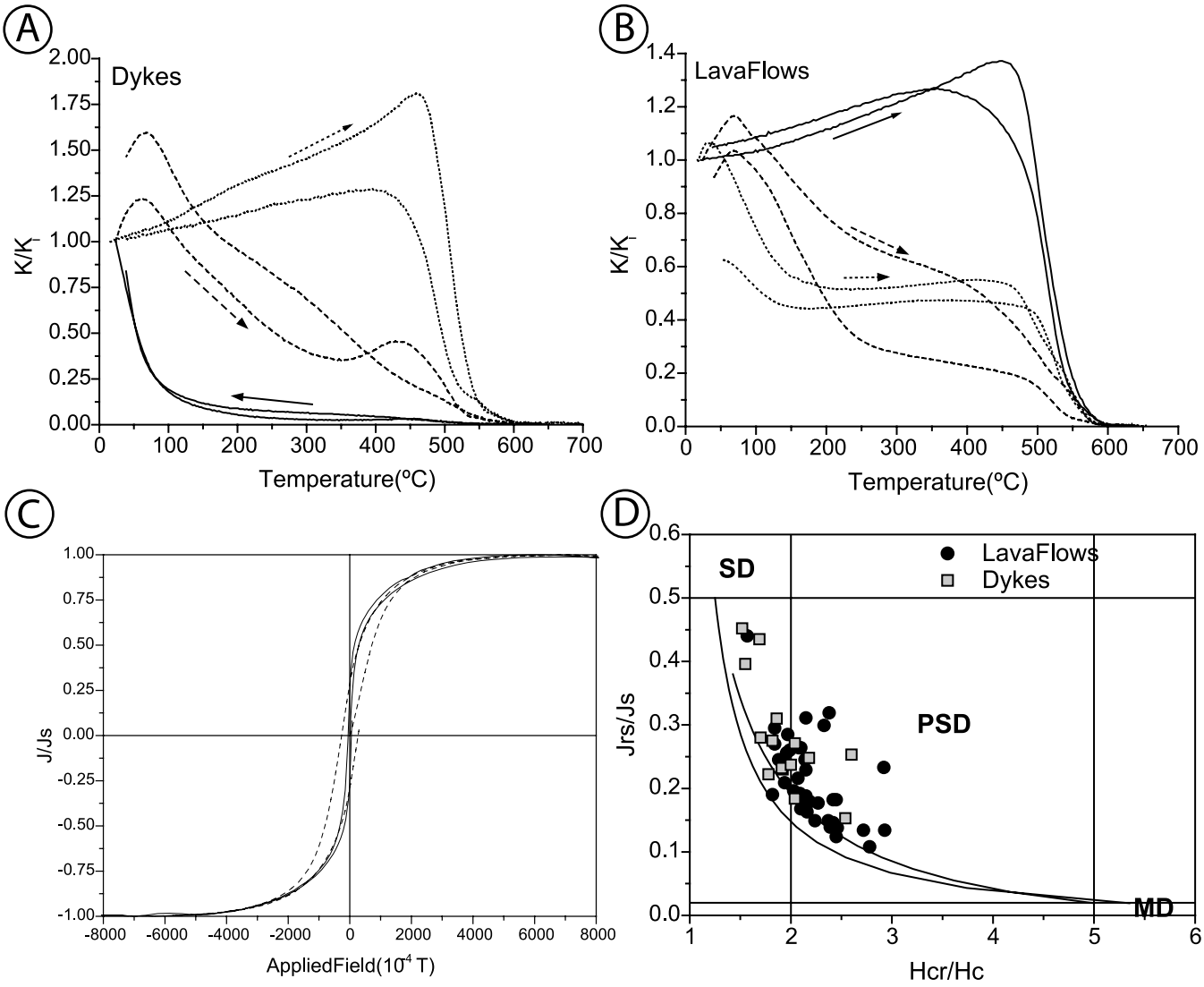

Figure 4. Rock magnetic properties of dykes and lava flows from S. Jorge. (a and b) Thermomagnetic experiments performed under Argon controlled atmosphere for dykes and lava flows, respectively. (c) Representative examples of hysteresis loops. (d) Day *et al.* (1977) diagram with limits and mixing curves proposed by Dunlop (2002) for titanomagnetites.

During heating, like for the $K(T)$ measurement, titanomaghemite becomes unstable and commonly inverts to a multiphase intergrowth with magnetite, ilmenite and/or hematite as probable end products (e.g. Readman & O'Reilly 1972; Özdemir 1987). Despite the possible occurrence of titanomaghemite, the persistence of the Hopkinson at the final steps of the cooling run indicates a slight oxidation of titanomagnetite, as corroborated by the SEM observations. The oxidation of titanomagnetite typically results from low-temperature oxidation that often arises during the final cooling stages, after lava emplacement (Wilson *et al.* 1968; Ade-Hall *et al.* 1971).

5.2 HIGH-FIELD EXPERIMENTS

Classical high-field experiments on lava flows and dykes (Fig. 4c) mostly show simple hysteresis loops. The presence of some wasp-waisted shapes indicates a possible mixture of different magnetic phases, possibly including superparamagnetic (SP) grains (Tauxe *et al.* 1996). After paramagnetic correction, the loops show saturation for applied fields below 300 mT. Such results point to the presence of a low-coercivity magnetic phase such as titanomagnetite. The Day diagram (Day *et al.* 1977), with limits of magnetic domain states redefined by Dunlop (2002) for titanomagnetite, indicates that the grain size of titanomagnetite mostly matches the transition between pseudo-single domain (PSD) and single domain (SD) magnetic states (Fig. 4d). This argues for the possible presence of stable remanent magnetization. Data show a shift to the right regarding envelope curves of SD + MD (multidomain) mixtures (Dunlop 2002), suggesting the presence of some minor amounts of SP particles and/or of a secondary component, likely titanomaghemite.

5.3 IRM

IRM of the analysed samples saturated for applied fields ranging from 200 to 300 mT (Fig. 5a). This confirms the presence of low-coercivity components, corroborating previous results indicating TM60 and TM0 as the main magnetic carriers.

Detailed cumulative log-Gaussian analyses (Robertson & France 1994) carried out on data from lava flows show the presence

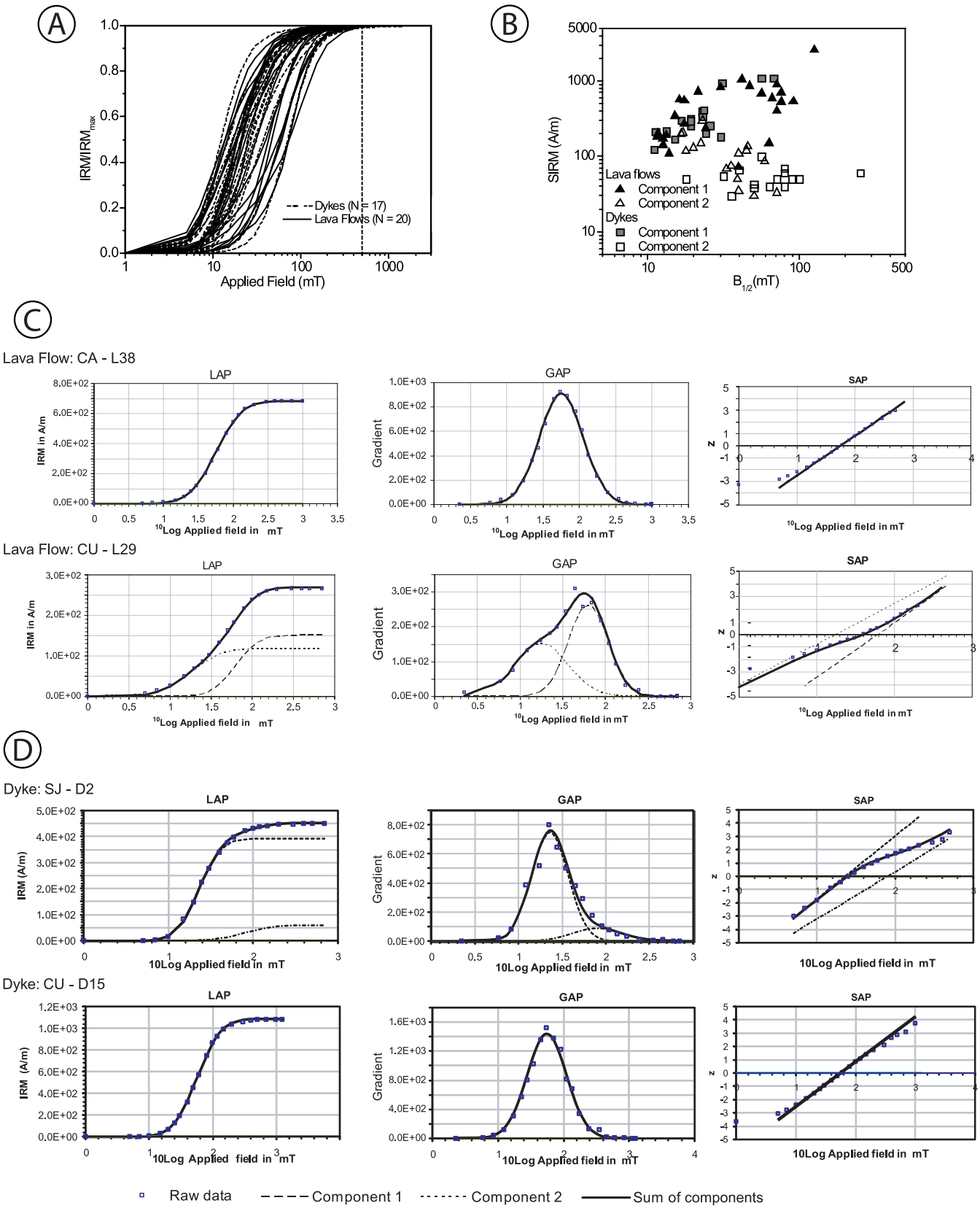

Figure 5. Results of Isothermal Remanent Magnetization (IRM) experiments. (a) IRM acquisition curves. (b) Saturated IRM (SIRM) versus Medium Destructive field ($B_{1/2}$) values. (c and d) Cumulative log-Gaussian analyses (Kruiver *et al.* 2001) for lava flows and dykes, respectively. LAP, Linear Acquisition Field; GAP, Gradient Acquisition Plot; SAP, Standardized Applied Field.

of a single ferromagnetic component for half of the samples, whereas two components were identified in the other half (Fig. 5c). For samples with two components, a magnetic phase dominates with 60–80 per cent of the signal. The main component presents medium destructive fields that range from 10 to 90 mT and a secondary one mostly between 30 and 90 mT (Fig. 5b).

Concerning dykes, the best fit of the log-Gaussian analysis indicates the presence of one or, in most samples, two components (Fig. 5d). The secondary component is responsible for less than 20 per cent of the remanence signal and appears for medium destructive fields around (70 mT), higher than for the main component (around 20 mT).

6 PALAEOMAGNETIC DATA

The evolution of the remanent magnetization during the demagnetization procedure is mostly similar in dykes and lava flows. A gradual decrease in magnetization is mainly observed from the thermal demagnetization until temperatures around 300°C, with the remaining signal (∼50 per cent) disappearing for higher temperatures, up to a maximum unblocking temperature of 500–580°C, depending on the samples (Figs 6a and d). During the AF treatment, 80 per cent of the magnetic signal disappeared for maximum fields ranging between 20 and 40 mT.

The main directions, as shown by the Zijderveld diagrams, mostly indicate the presence of a single ChRM component for temperatures and fields above 300°C and 10–20 mT, respectively. This component, accurately determined by principal component analysis (Kirschvink 1980), is quite similar for both types of demagnetization techniques, within each lava flow or dyke. For low temperatures and AF intensities, minor variations of the main direction probably reflect the presence of a viscous magnetization component. Mean ChRMs directions (Table 1) show negative inclinations for the eastern part of the island (23 of the 24 lava flows and 11 dykes), and positive for the central and western domains of the island (14 lava flows and nine dykes).

7 DISCUSSION

7.1 Palaeomagnetic interpretation

Mean ChRMs were determined for a cut-off angle of 45° (e.g. Vandamme 1994; Biggin *et al.* 2008; Johnson *et al.* 2008) applied for the palaeopole latitude to eliminate intermediate polarity directions acquired during a reversal event. These data highlight the presence of five intermediate directions recorded in flows and dykes of the eastern part of the island (see section later on magnetostratigraphy). Normal and reversed palaeomagnetic polarities correspond to distinct geographic domains of the island. The lava flows and dykes from central and western parts of S. Jorge present only normal polarity, with a mean ChRM of 357.7°/52.3° for 23 sites, with $k = 67$ and $\alpha_{95} = 3.7°$. In the eastern part, only reversed polarity was found, with a mean ChRM of 188.9°/–40.7° for 32 sites, with $k = 21$ and $\alpha_{95} = 5.7°$ (Fig. 7a and Table 1). According to the available geochronological results for S. Jorge (Féraud *et al.* 1980; Hildenbrand *et al.* 2008), the onshore volcanic activity includes Matuyama (reversed polarity) and Brunhes (normal polarity) geomagnetic chrons. There is a perfect agreement between the obtained and expected polarity from the most recent geochronological data (Hildenbrand *et al.* 2008).

To check if the distributions with reverse and normal polarities share a common direction, the reversal test of McFadden & McElhinny (1990) was applied to our mean site ChRMs. It fails with an observed angle $\gamma_o = 13.9°$, higher than the critical value $\gamma_c = 7.4°$. A deficient time covering of the palaeosecular variation of lava flows (PSVL) is a possible explanation for such failure. The 58 mean ChRMs encompass a total time interval of approximately 1 Myr, which is 10 times larger than the 10^5 yr assumed for correctly averaging out the PSVL (Johnson & Constable 1995); however, the mean ChRMs are concentrated in different periods within this interval. The lava pile recording only reversed polarity at S. João sea cliffs (21 lava flows) encompasses a mean time interval of 1.16×10^5 yr, between 1.323 ± 0.021 and 1.207 ± 0.017 Ma, with an apparent regular distribution of the sampled flows in time, i.e. a flow every 6 kyr on average (Fig. 8). For such periodicity and regularity, a reasonable evaluation of the PSVL is expected. At the Cubres site, only the age of a lava flow from the base of the pile is known, and it is therefore not possible to discern if PSVL is correctly averaged for this section.

7.2 Dyke emplacement effects on lava flows

Volcanic edifices commonly show the lateral collapse of significant volumes of material, such as observed along the Hawaiian ridge, in French Polynesia, around the Canary Archipelago, or at Reunion Island (e.g. Moore *et al.* 1989; Gillot *et al.* 1994; Day *et al.* 1999; Owen *et al.* 2000; Clouard *et al.* 2001; Hildenbrand *et al.* 2003, 2004, 2006; Merle & Lénat 2003; Quidelleur *et al.* 2008; Boulesteix *et al.* 2012). Such landslides are often associated with deep-reaching listric faults, basal detachment and gravitational loading of the flanks (Walker 1988; Borgia *et al.* 2000; Morgan & Clague 2003; Le Corvec & Walter 2009). Gradual flank collapses commonly lead to block sliding and rotations, with consequences regarding palaeomagnetic data and interpretation (e.g. Riley *et al.* 1999; Delcamp *et al.* 2010). Comparing the reversed ChRM of lava flows and dykes in the S. João area, a 13.5° difference in dip appears: 189.8°/–35.6° for 21 flows ($\alpha_{95} = 6.8°$), and 179.1°/–46.5° for nine dykes ($\alpha_{95} = 5.1°$). The low negative inclination of lava flows ChRM suggests a tilting of the western part of the old lava pile towards the SW. Such tilting disagrees with the hypothesis of block rotations induced by SW-dipping listric faults. Sliding along such faults should have produced an increase of the ChRM inclination by tilting towards the internal part of the island, i.e. towards the NE. However, if the S. João lava pile were the NNE border of a main ridge presently greatly eroded, NE-dipping listric faults could be responsible for the origin of the tilting.

Concerning 'reversed' dykes, we know that: (i) the great majority of the dykes (nine of 11) are subvertical and the two remaining dip 75° and 84° towards SW and NE, respectively; they all show similar ChRMs; (ii) local dip-slip movements along dykes and fault planes have been evidenced in this study; (iii) dykes cutting the lava flows have an NNW–SSE direction and (iv) the reversal test of McFadden & McElhinny (1990) becomes positive (with $\gamma_o = 5.9°$ for $\gamma_c = 6.6°$) when performed without the lava flows carrying a reversed polarity. These results point to the stability of dykes since emplacement, in contrast with the host rock lava flows.

Magma overpressure can be responsible for the emplacement of significant amounts of intrusions, which are able to laterally push, and thermally and mechanically damage the host rocks (Lyakhovsky *et al.* 1997; Rubin & Pollard 1988; Mériaux *et al.* 1999; Silva *et al.* 2006a,b, 2008). Dyke emplacement thus can favour flank

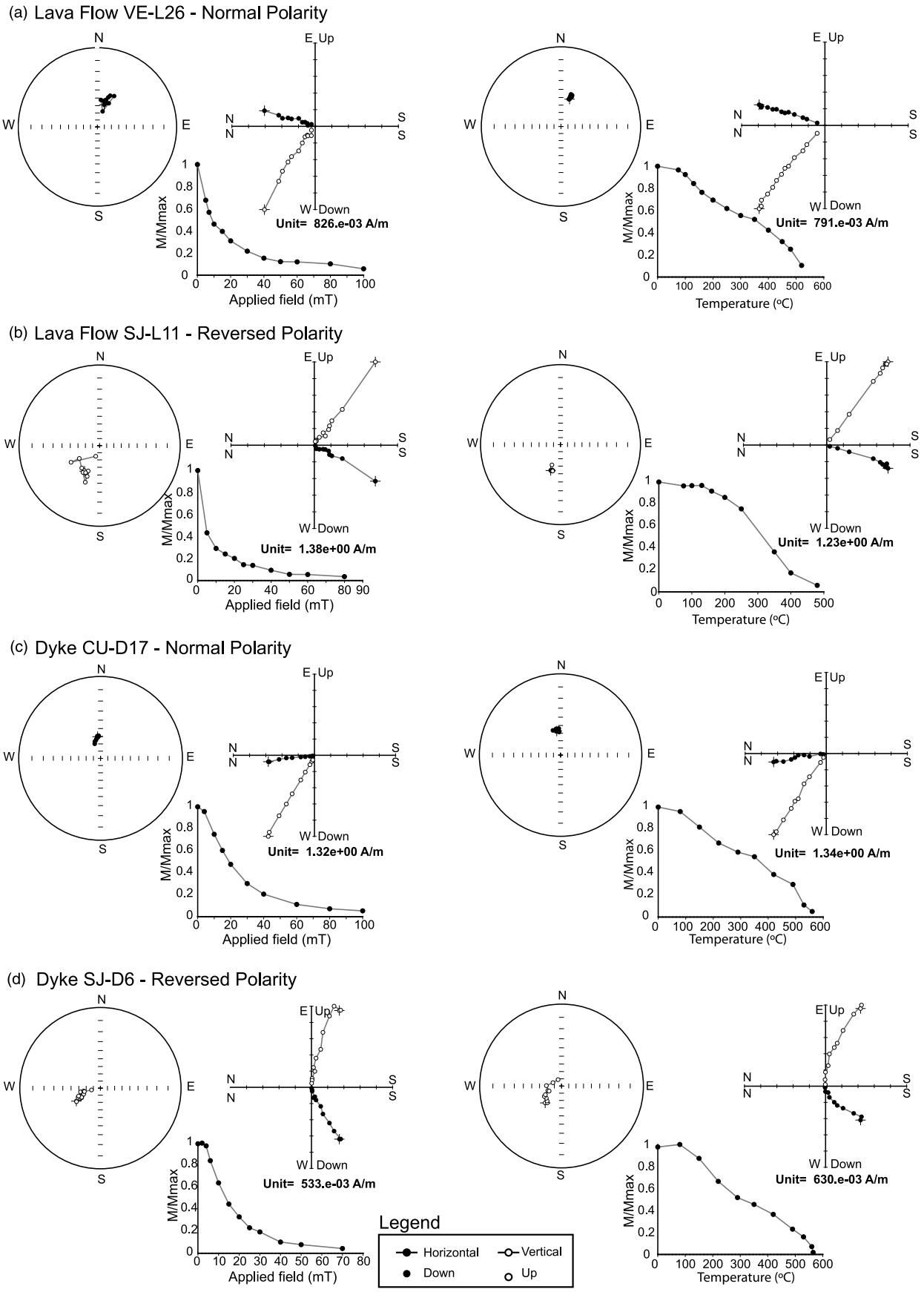

Figure 6. (a–d) Examples of the direction and intensity evolution of the remanent magnetization during alternating field (AF) and thermal demagnetization procedures, and stereographic projections and remanence decay curves.

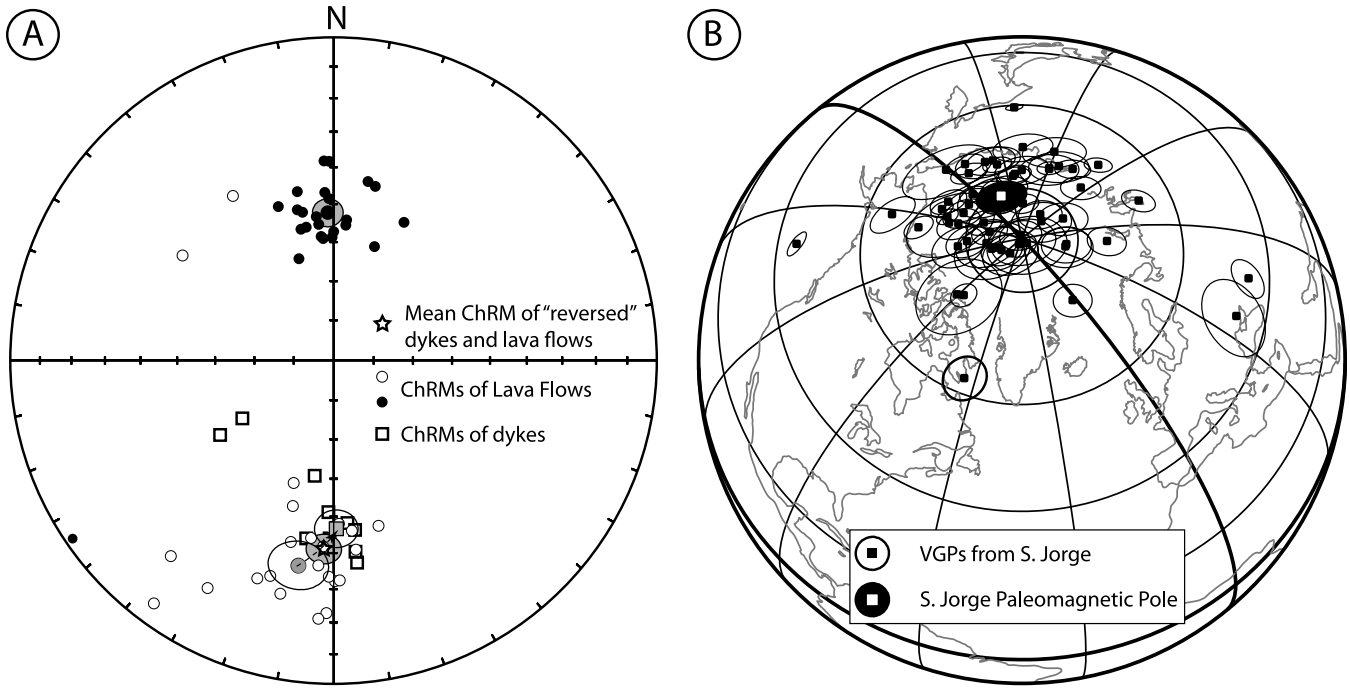

Figure 7. (a) Stereographic projection of the ChRM mean direction per lava flow and dyke. Full and open symbols correspond to lower and upper hemispheres, respectively. Mean directions presented with confidence zone α_{95}. Arrow indicates the sense of dip correction for lava flows with reverse polarity. (b) Globe representation of the VGPs obtained for S. Jorge, and the resulting mean pole after 45° cut-off application. All poles are presented with confidence zone A_{95}.

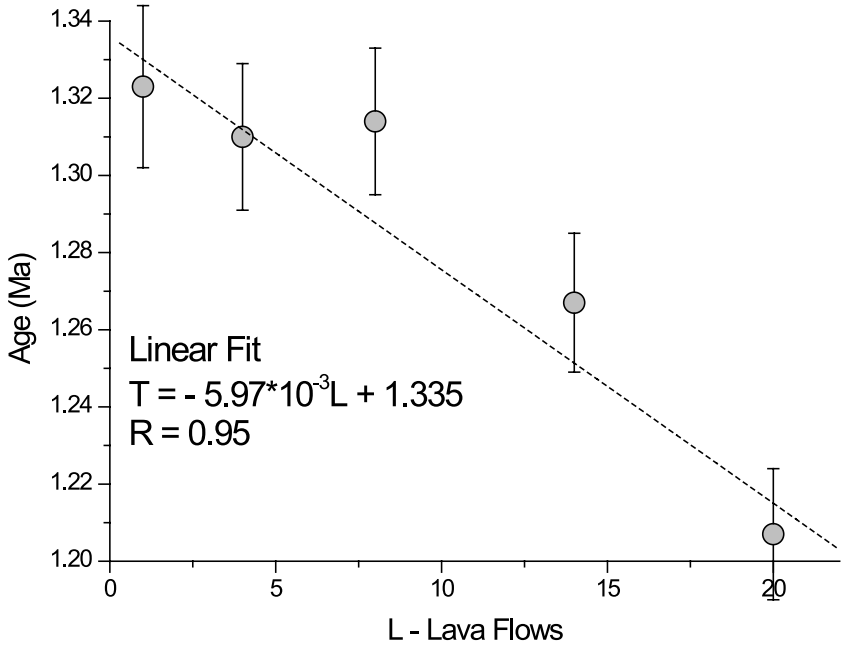

Figure 8. Sampled lava flows in stratigraphical order (circles correspond to dated flows—this study and Hildenbrand *et al.* 2008) along the S. João section, as a function of the known ages in Ma. Slope of linear fit ($R^2 = 0.95$) indicates approximately 6 kyr between each sampled successive flow.

instability in volcanic edifices, mostly due to changes in the static equilibrium between the volcanic edifice loading and lithostatic pressure, and through an increase of the pore fluid pressure that promotes failure (e.g. Elsworth & Voight 1992; Battaglia *et al.* 2011). The palaeomagnetic results suggest that the tilting of the S. João lava pile towards the WSW was promoted by short-term effects related to the emplacement of the NNW–SSE dykes, e.g. inflation and deformation of the central part of the edifice during repeated upward magma ascent. Although the S. João lava pile apparently did not collapse as a whole, deformation of the edifice promoted by dyke emplacement may have favoured the destabilization of the more distal parts of the succession. Such a mechanism could explain the genesis of a steep lateral topographic contact between the old succession and the younger lava piles a few kilometres west of the S. João site, as pointed out by Hildenbrand *et al.* (2008).

Applying a classical dip correction of 13.5° (angular difference between ChRMs of 'reversed' lava flows and dykes; see Fig. 7a) to the flows of S. João section, the resulting ChRM direction for 30

of the lava flows and dykes with reverse polarity appears now as 179.1°/–46.5°, with $k = 31$ and $\alpha_{95} = 4.8°$. The reversal test after this tilt correction is now positive with $\gamma_o = 5.9°$ for $\gamma_c = 6.3°$. This would not happen if we had applied a dip correction of 13.5° to the dykes, to have a ChRM direction coherent with that of the lava flows. This justifies our choice of the applied correction.

At the Cubres section, a similar palaeomagnetic direction appears between lava flows and dykes, and between WNW–ESE and ENE–WSW dyke swarms. The coincidence in palaeomagnetic orientation of all of the data from the island (after untilting of the reversed S. João lava flows) indicates that the other sections were not significantly affected by dyke emplacement.

7.3 Palaeopole and palaeomagnetic field

Again applying a cut-off angle of 45°, the mean direction becomes 358.5°/49.0° for 53 sites with $k = 39$ and $\alpha_{95} = 3.2°$ after untilting of the reversed flows. Such results correspond to mean palaeomagnetic pole with Plat = 81.3°N, Plong = 160.7°E, $K = 33$ and $A_{95} = 3.4°$ (Fig. 7b). According to McFadden & Lowes (1981), the pole we estimated is statistically coincident with that of Johnson *et al.* (1998) estimated from ChRMs on the S. Miguel island (Plat = 82.2°N and Plong = 157.1°E, for 26 lava flows with $K = 41$ and $A_{95} = 4.4°$). It is also close to the result of Chauvin *et al.* (1990) for a similar period in French Polynesia, Plat = 82.3°N and Plong = 202.6°E, with $K = 112$ and $A_{95} = 4.9°$ (obtained for a sequence of nine lava flows before the first intermediate direction). The angular standard deviation of the PSVL about the geographic axis gives a value of 17.2° (value obtained after subtraction of the within-site dispersion according to eq. (4) of Johnson *et al.* 2008). 17.2° is within the range of values (14.3°–18.1°) expected for the latitude of S. Jorge by the Model G of McFadden *et al.* (1988), with shape parameters recalculated by Biggin *et al.* (2008) from PSVL data selection of Johnson *et al.* (2008). This suggests that our data average out the secular variation. Despite our palaeomagnetic pole being statistically well determined, its mean latitude has a value lower by 8.7° than expected by the Geocentric Axial Dipole (GAD) assumption.

Rock magnetic anisotropy can affect the palaeomagnetic direction, with a consequent departure from the local geomagnetic field direction. Such effects have been evidenced in sediments and sedimentary rocks (e.g. Jackson *et al.* 1991; Tauxe 2005; Borradaile & Almqvist 2008), as well as in deformed igneous rocks (e.g. Reisinger *et al.* 1994). To check the possible influence of the anisotropy on the palaeomagnetic directions, AMS measurements were performed on the great majority of S. Jorge lava flows and dykes. The results essentially indicate the presence of low anisotropy ($P' < 1.1$), with a variable shape of the AMS ellipsoid (Fig. 9). The dykes show a coherent pattern, with a magnetic foliation mostly parallel to the dyke plane (Fig. 9b). Regarding lava flows, the general picture is more complex (Fig. 9a), with often a scattered distribution of the principal axes. Comparison of AMS and palaeomagnetic results shows that normal polarity dykes and flows do not carry similar magnetic fabric but have almost parallel palaeomagnetic directions. Therefore, the orientation of the latter is not related to the magnetic anisotropy of these rocks.

Evidences for a systematic departure of recent palaeopoles from the GAD simple model have commonly been found by several authors who develop geomagnetic field models. These encompass time periods of different scales: from historical to present times (e.g. Yukutake 1971; Jackson *et al.* 2000); for the last kyr (e.g. Korte & Constable 2005; Korte *et al.* 2009); for the last 5 Myr (Quidelleur *et al.* 1994; Johnson & Constable 1997; McElhinny & McFadden 1997; Carlut & Courtillot 1998; Johnson *et al.* 2008); for several tens/hundreds of Myr (e.g. Kent & Smethurst 1998; McFadden *et al.* 1988; Van der Voo & Torsvik 2001; Biggin *et al.* 2008). The reason for such differences is generally ascribed to the presence of non-dipole fields (mostly quadrupole and octupole axial terms), which are responsible at mid-latitudes for long-term differences of GAD by approximately 4° (Johnson *et al.* 2008) to 7.5° (Van der Voo & Torsvik 2001). Regarding the mean palaeomagnetic poles from Canary and Madeira archipelagos (also in the North Atlantic), latitudes of 84.9° are observed within the last 2 Myr (Carracedo & Soler 1995; Quidelleur & Valet 1996), and even lower values of 81.3° (Watkins 1973) or 77.8° (Storetvedt *et al.* 1979) for the last 20 Myr. A global tilting of the Azores, Canary and Madeira archipelagos or a systematic tilting of all the islands towards a similar direction cannot be reasonably envisaged. Therefore, we interpret the shallow latitude here presented as the one that can be inferred from Johnson *et al.* (1998) for S. Miguel (82.2°), as a result of non-dipolar components.

7.4 Magnetostratigraphy and Cobb Mountain Subchron

The S. João lava pile was mostly built up between 1.323 ± 0.021 and 1.207 ± 0.017 Ma (Hildenbrand *et al.* 2008). From bottom to top, the ChRMs mostly show a declination varying between the azimuths 170° and 200°, except for the uppermost lava flows (Fig. 10). Regarding inclinations, oscillations between –50° and –10° were observed in the lowermost lava flows (values mostly around –45°). For part of the eight uppermost flows (age around 1.207 Ma), the ChRM shows a different behaviour, characterized by strong variations of both declination and inclination.

The virtual geomagnetic poles (VGP) for the bottom part of the section, including SJ-L17, are mainly clustered around high latitudes (Figs 10 and 11), whereas intermediate latitudes over the Pacific Ocean are obtained for lava flows SJ-L21, SJ-L22 and SJ-L24. The age of flow SJ-L21 (1.207 ± 0.017 Ma) matches the age expected for Cobb Mountain normal polarity subchron, as recently redefined in the interval 1182–1208 ka by Channell *et al.* (2008), and is consistent with several other estimates derived from distinct dating methods (Shackleton *et al.* 1990; Turrin *et al.* 1994; Berggren *et al.* 1995; Renne *et al.* 1998; Horng *et al.* 2002).

Cobb Mountain is a worldwide short duration normal polarity subchron (e.g. Mankinen *et al.* 1978; Sueishi *et al.* 1979; Hsu *et al.* 1990; Clement 2000) that occurred on a period of 26–35 kyr (Channell *et al.* 2002, 2008; Channell & Raymo 2003) during the Matuyama reversed chron (e.g. Watkins 1968; Foster & Opdyke 1970; Chauvin *et al.* 1990; Clement 1992; Clement & Martinson 1992). This subchron has been first established in the Clear Lake Volcanics (Mankinen *et al.* 1978), and recognized later in sedimentary rocks from ODP and DSDP cores (e.g. Hsu *et al.* 1990; Clement 1992, 2000; Abrahamsen & Sager 1994). Due to its short duration, records of this subchron in lava flows are very scarce. Lava flows from Clear Lake Volcanics and Coso Range contribute with a total of seven significant palaeomagnetic poles (Mankinen *et al.* 1978, 1981; Mankinen & Grommé 1982). Along a volcanic sequence at Tahiti (in the Punaruu Valley), Chauvin *et al.* (1990) found 14 lava flows with intermediate directions for an age around 1.1 Ma, and proposed the Cobb Mountain as the geomagnetic subchron responsible for such records. From a re-evaluation of geochronological results, Singer *et al.* (1999) suggested that Punaruu Valley and Coso Range data record a different event, approximately 80 kyr younger than Cobb Mountain, and denominated as the Punaruu event.

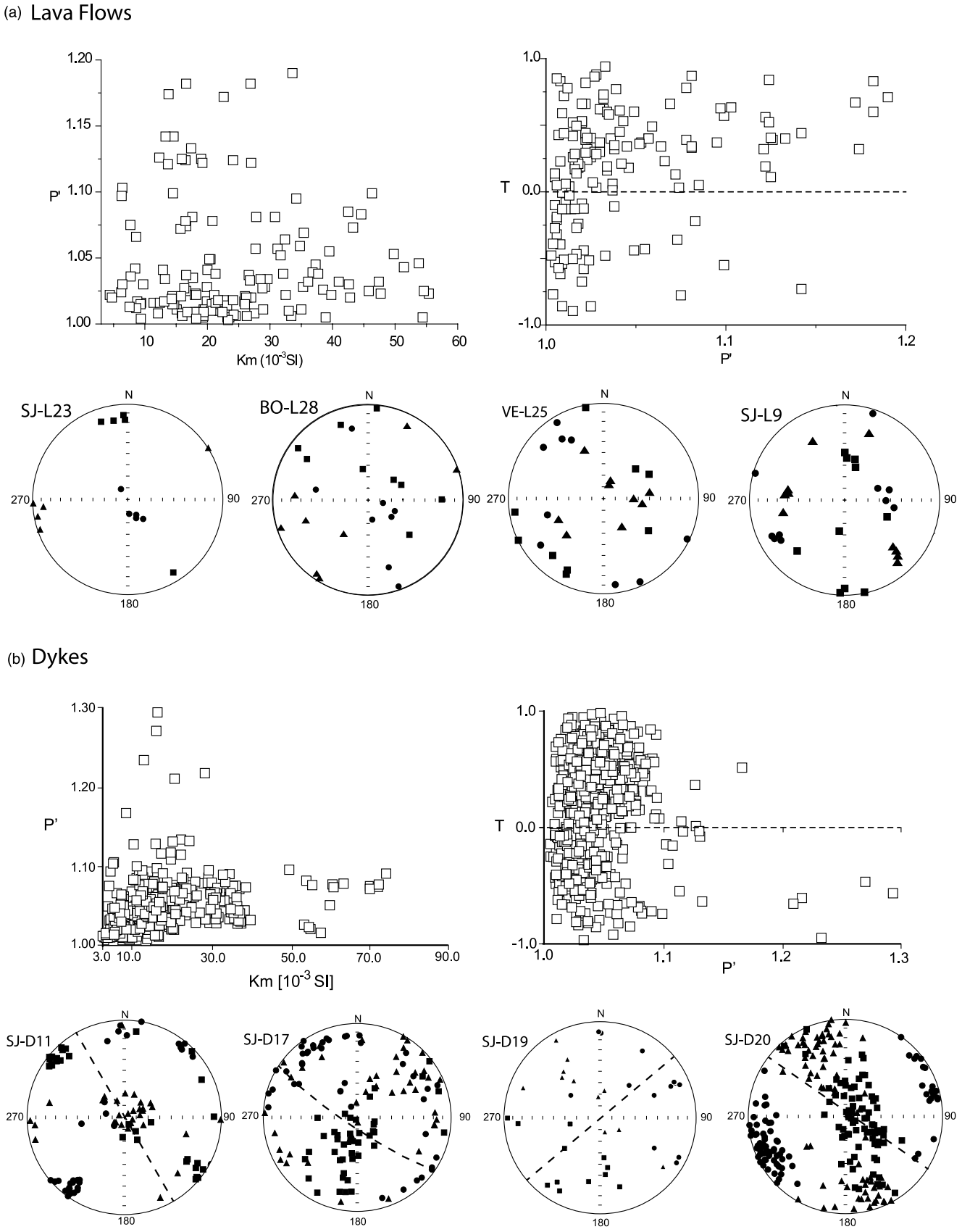

Figure 9. Graphical presentation of the main AMS results from (a) lava flows and (b) dykes. Stereographic projections (lower hemisphere) with indication of the maximum K_1 (squares), intermediate K_2 (triangles) and least K_3 (circles) principal magnetic susceptibility axes. Dashed line, dyke plane; P', corrected degree of anisotropy; T, shape parameter; K_m, bulk magnetic susceptibility.

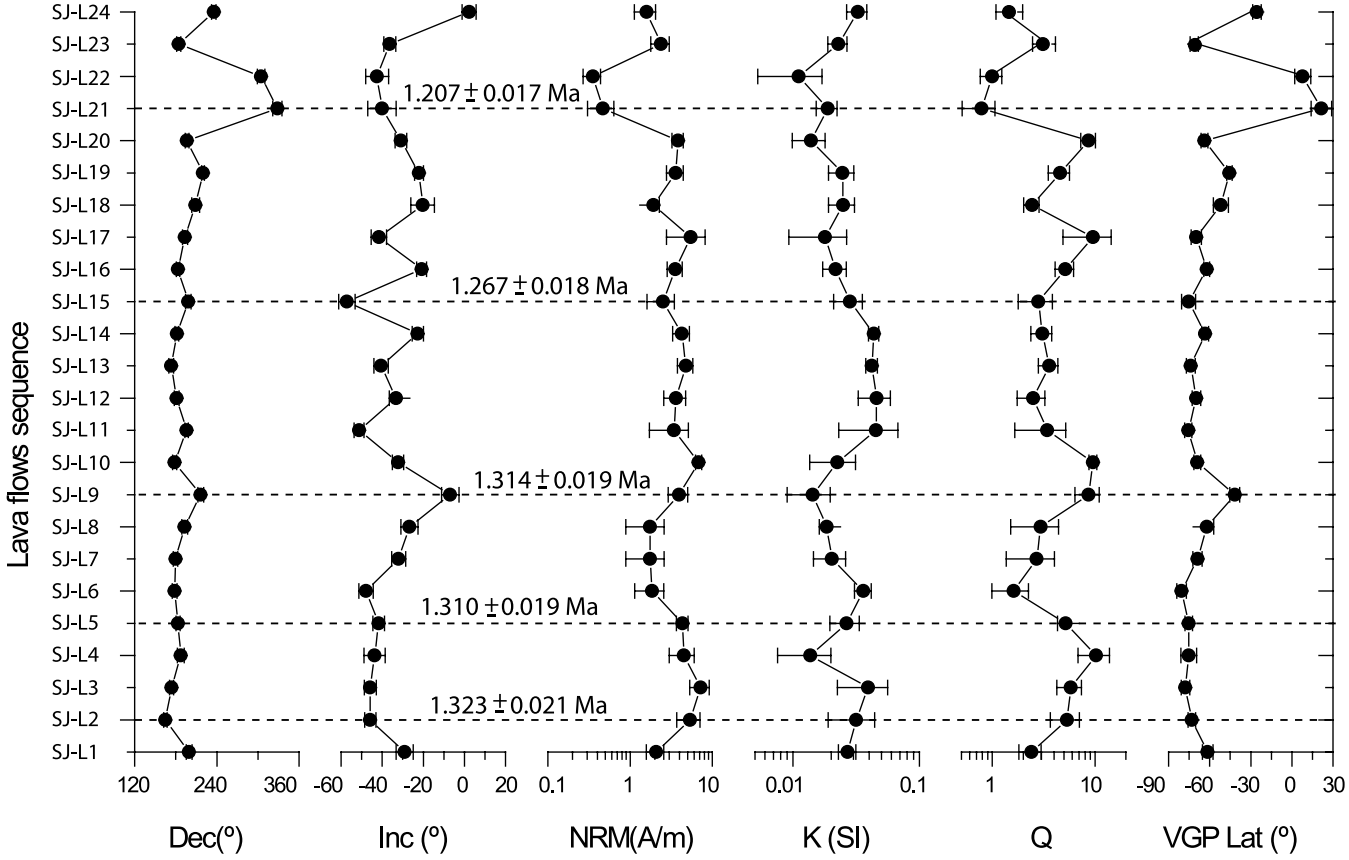

Figure 10. Magnetostratigraphy along the S. João section, with indication of the available ages. All mean values with error bars. Dec and Inc, declination and inclination of the ChRM; NRM, natural remanent magnetization intensity; *K*, bulk susceptibility; *Q*, Koenigsberger ratio (considered for an external field of 40 μT); VGP Lat, latitude of the virtual geomagnetic pole.

Accordingly, volcanic rocks that recorded Cobb Mountain Subchron would then be limited to the Clear Lake Volcanics, with a total of only five palaeomagnetic results. However, due to the similarity of the Punaruu data with marine Cobb Mountain Subchron records, Clement (2000) argued for an attribution of Punaruu data to the Cobb Mountain Subchron.

According to ODP/DSDP data reported by Clement (2000), before the transition from reversed to normal polarity with different swings (D, E and F) across the Pacific Ocean (Fig. 11), the magnetic pole, initially centred at the south geographical pole (A), swung twice, initially towards South Africa (B) and later towards southwest Australia (C). The transition from normal (G) to reversed (L) polarity was also characterized by swings in central Asia (H), northern Canada (I), South Africa (J) and southwest South America (K). SJ-L17, SJ-L18 and SJ-L19 palaeomagnetic data from S. João show a gradual migration of the VGPs from the southern pole towards South America (compare Figs 10 and 11 with Table 1). SJ-L20 VGP is quite similar to the SJ-L17 VGP, and most probably records the return of a swing towards South America. The record of this swing by these lava flows is mostly responsible for a skewed distribution of the ChRMs towards SW (see Fig. 7a). Similar pole locations have been obtained for the ODP site 839 (Abrahamsen & Sager 1994; Clement 2000), possibly related to a preliminary stage of the transition Reversed–Normal. SJ-L21 and SJ-L22 could correspond to swing D, and SJ-L24 to swing K. SJ-L23 likely corresponds to a reversed stage between the different swings. Such a repartition during the Cobb Mountain Subchron is in agreement with the duration of the subchron and the estimated mean interval between successive individual flows (6 kyr—see Fig. 8). The age reported here for lava flow SJ-L21 (1.207 ± 0.017 Ma), which is the lowermost flow recording a VGP with positive latitudes, is in agreement with the age of 1.208 Ma (Channell *et al.* 2008) expected for the beginning of the period with normal polarity, reinforcing the hypothesis that SJ-L21 was emplaced during the transition from reversed to normal polarity of the Cobb Mountain Subchron. Furthermore, it reinforces the validity of the age previously obtained on fresh-separated groundmass with the Cassignol–Gillot technique (Hildenbrand *et al.* 2008). The intermediate latitudes are here associated with relatively low values of the Koenigsberger ratio *Q* (Fig. 10). Low *Q* values are correlated with low remanence values that likely result from low intensity of the Earth's magnetic field, as reported by Channell *et al.* (2008) for the Cobb Mountain Subchron.

Moreover, two of the S. João dykes (SJ-D4 and SJ-D6) show intermediate directions in close agreement with swing D, suggesting that these two dykes could belong to an intrusive episode with an age around 1.207 Ma.

7.5 Timing of dyke emplacement

The dyke swarms in S. Jorge correspond to three main orientations and two palaeomagnetic polarities, which correlate with different spatial domains within the island. In the eastern part of the island, the dykes are preferentially oriented NNW–SSE and present reversed or intermediate magnetic polarity, consistent with the corresponding host lava flows. In the central-western domain, most dykes are

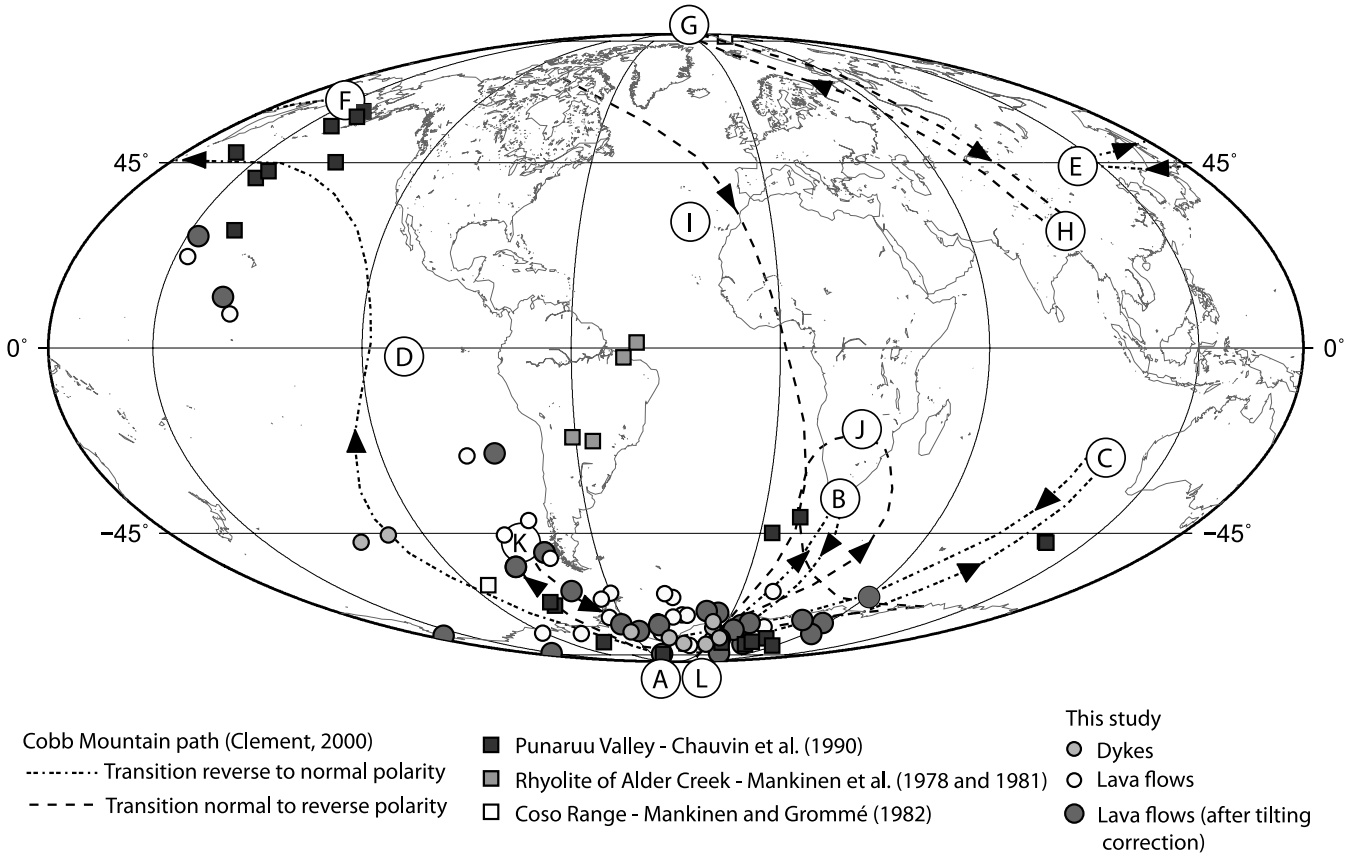

Figure 11. Equal area Mollweide projection showing the VGPs during part of the Matuyama chron. Fit of the sequential presentation of VGP paths for Cobb Mountain Subchron, as proposed by Clement (2000), and supported by palaeomagnetic results of ODP/DSDP cores (see text).

subparallel to the island elongation (WNW–ESE) and a few dykes strike ENE–WSW, all presenting normal magnetic polarity. Such results show that dykes intruded the eastern and central-western domains of the island along different preferential orientations at distinct times: (i) NNW–SSE striking dykes intruded the eastern part of the island during the Matuyama Chron; (ii) Younger WNW–ESE and ENE–WSW striking dykes intruded the central-western domain of the island during the Brunhes Chron.

To the present, the available geochronological results for S. Jorge Island (Féraud *et al.* 1980 and Hildenbrand *et al.* 2008) concerned only lava flows. The only indication for dykes, from the younger age of the host rock, was their maximum age. The reversed polarity obtained on NNW–SSE dykes constrains their emplacement age to a time window between *ca.* 1.2 and 0.79 Ma, the age of the Matuyama–Brunhes transition (Quidelleur *et al.* 2003). The other dyke swarm (WNW–ESE and ENE–WSW) definitely belongs to a more recent history.

7.6 Dyke directions and regional stress field

Dyke orientations have commonly been used to get insight into the regional stress field, because they either propagate perpendicular to the direction of minimum compression that is the direction of opening (e.g. Rubin 1995; Curewitz & Karson 1998; Mériaux & Lister 2002; Silva *et al.* 2010) or they are intruded along pre-existing fractures.

Considering the NUVEL-1A kinematic model (DeMets *et al.* 1994), the three tectonic plates around the Azores Plateau show a steady kinematic behaviour during the last million and half years. The velocity of the Eurasian Plate relative to a fixed African Plate is of *ca.* 4.4 mm yr^{-1} along N70°, and the velocity of the African Plate relative to a fixed North American Plate is of 20 mm yr^{-1} along N284°. This kinematics is consistent with a right-lateral transtensional regime at the present Europe–Africa plate boundary on the Azores Plateau. The average far-field stress regime associated with this kinematics yields a minimum principal stress component along the NNE–SSW direction (e.g. Madeira & Ribeiro 1990; Lourenço *et al.* 1998; Miranda *et al.* 1998).

This stress pattern can justify the observed dyke directions in S. Jorge. The NNW–SSE system is preferentially associated with left-lateral strike-slip (e.g. Buforn *et al.* 1988; Borges *et al.* 2007; Dias *et al.* 2007). The WNW–ESE system could be associated with normal faulting, and with the most recent volcanic activity: the 1956/1957 Capelinhos eruption on Faial Island (e.g. Machado *et al.* 1962), and 1998/1999 Serreta submarine eruption on Terceira Island (Luis *et al.* 1999; Gaspar *et al.* 2003). The coincidence of fault and dyke directions locally observed on S. Jorge suggests that dykes have intruded major pre-existing fractures.

This work also presents a case for age/location relations of the two volcano-tectonic directions on S. Jorge. The eastern area of the island is dominated by the NNW–SSE system which was magmatically active during the end of the Matuyama Chron, whereas during the Brunhes Chron younger dykes intruded the central-western domain of the island along the WNW–ESE direction, and less significantly along ENE–WSW.

The intrusion of magma along pre-existing fractures, although with distinct timing and location of intrusion, could simply reflect

a slight shift of the magmatic source towards the S, following the Azores hotspot migration (Cannat *et al.* 1999). However, the dynamics in the Azores is so complex that it would be logical to also invoke other possibilities such as a small change of the stress field (DeMets *et al.* 1994; Luis *et al.* 1994; Hildenbrand *et al.* 2008).

8 CONCLUSIONS

The palaeomagnetic study of S. Jorge Island led to relevant results. The new obtained palaeomagnetic pole (Plat = 81.3°N, Plong = 160.7°E, $K = 33$ and $A_{95} = 3.4°$, from 38 lava flows and 20 dykes showing normal or reversed polarity) has important implications on the knowledge of the Earth's palaeomagnetic field, confirming previous indications of the effect of non-dipolar components inferred from palaeomagnetic data from S. Miguel Island, and Canary and Madeira archipelagos. Very few reliable VGPs from volcanic rocks were known for the Cobb Mountain Subchron before this work. Our new data set adds 10 new VGPs that record several swings of the Earth's magnetic pole for this subchron and constrains from accurate unspiked K/Ar dating on fresh-separated groundmass the beginning of the period with normal polarity at *ca.* 1.207 ± 0.017 Ma, in agreement with recent works (Channell *et al.* 2008). Volcano flank instability inferred for S. Jorge does not seem to be related to classical sliding, and seems to be the result of dyke intrusion. Palaeomagnetic data from dykes yield key information about the timing and conditions of intrusion of the two main populations of dykes.

The presented data underline the potential of such studies in complex areas, like volcanic islands. It will be therefore of high interest to extend similar research on the other Azores islands, particularly on those where lava flows were or are still the subject of geochronological dating, like Faial, Pico or Terceira.

ACKNOWLEDGMENTS

This study was funded by FCT (Portugal), through the research projects TEAMINT (POCTI/CTE/48137/2002), EVOLV (PTDC/CTE-GIN/71838/2006) and MEGAHAZARDS (PTDC/CTE-GIX/108149/2008), and by Instituto Dom Luiz (IDL) and Centro de Geofísica de Évora. Special thanks are due to Nuno Lourenço and Miguel Miranda for fruitful discussions regarding the Azores geodynamic setting. We also thank José Mirão for assistance during SEM analyses at Centro Hércules. We are grateful to Rob Van der Voo, an anonymous Reviewer and the Editor Andy Biggin for their helpful comments. Finally, we thank Fiona McMillan for correcting the English.

REFERENCES

Abrahamsen, N. & Sager, W., 1994. Cobb Mountain geomagnetic polarity event and transition in three deep-sea sediment cores from the Lau Basin, *Proc. ODP, Sci. Results,* **135,** 737–762.

Ade-Hall, J.M., Palmer, H.C. & Hubbard, T.P., 1971. The magnetic and opaque petrological response of basalts to regional hydrothermal alteration, *Geophys. J. R. astr. Soc.*, **24,** 137–174.

Battaglia, M., Di Baria, M., Acocella, V. & Neri, M., 2011. Dike emplacement and flank instability at Mount Etna: Constraints from a poro-elastic-model of flank colapse, *J. Volc. Geotherm. Res.*, **199,** 153–164.

Beier, C., 2006. The magmatic evolution of oceanic plateaus: a case study from the Azores, *PhD thesis*, University of Kiel, Germany.

Berggren, W.A., Hilgen, F.J., Langereis, C.G., Kent, D.V., Obradovich, J.D., Raffi, I., Raymo, M.E. & Shackleton, N.J., 1995. Late Neogene chronology: New perspectives in high-resolution stratigraphy, *Bull. Geol. Soc. Am.*, **107,** 1272–1287.

Biggin, A.J., van Hinsbergen, D.J.J., Langereis, C.G., Straathof, G.B. & Deenen, M.H.L., 2008. Geomagnetic secular variation in the Cretaceous Normal Superchron and in the Jurassic, *Phys. Earth planet Inter*., **169,** 3–19.

Borges, J.F., Bezzeghoud, M., Buforn, E., Pro, C. & Fitas, A., 2007. The 1980, 1997 and 1998 Azores earthquakes and some seismo-tectonic implications, *Tectonophysics*, **435,** 37–54.

Borgia, A., Delaney, P.T. & Denlinger, R.P., 2000. Spreading volcanoes, *Annu. Rev. Earth planet. Sci.*, **28,** 539–570.

Borradaile, G.J. & Almqvist, B.S., 2008. Correcting distorted paleosecular variation in late glacial lacustrine clay, *Phys. Earth planet. Inter.*, **166,** 30–43.

Boulesteix, T., Hildenbrand, A., Gillot, P.Y. & Soler, V., 2012. Eruptive response of oceanic islands to giant landslides: new insights from the geomorphologic evolution of the Teide–Pico Viejo volcanic complex (Tenerife, Canary), *Geomorphology,* **138,** 61–73, doi:10.1016/j.geomorph.2011.08.025.

Buforn, E., Udías, A. & Colombás, M.A., 1988. Seismicity, source mechanisms and tectonics of the Azores-Gibraltar plate boundary, *Tectonophysics*, **152,** 89–118.

Cannat, M. *et al.*, 1999. Mid-Atlantic Ridge-Azores hotspot interactions: along-axis migration of a hotspot-derived event of enhanced magmatism 10 to 4 Ma ago, *Earth planet. Sci. Lett.*, **173,** 257–269.

Carlut, J. & Courtillot, V., 1998. How complex is the time averaged geomagnetic field over the last 5 million years? *Geophys. J. Int.*, **134,** 527–544.

Carracedo, J.C. & Soler, V., 1995. Anomalously shallow palaeomagnetic inclinations and the question of the age of the Canarian Archipelago, *Geophys. J. Int.*, **122,** 393–406.

Cassignol, C. & Gillot, P.-Y., 1982. Range and effectiveness of unspiked Potassium-argon dating: experimental groundwork and applications, *Numerical Dating in Stratigraphy*, pp. 159–179, ed. Odin, G.S., Wiley, Chichester.

Channell, J.E.T. & Raymo, M.E., 2003. Paleomagnetic record at ODP Site 980 (Feni Drift, Rockall) for the past 1.2 Myrs, *Geochem. Geophys. Geosyst.*, **4,** doi:10.1029/2002GC000440.

Channell, J.E.T., Mazaud, A., Sullivan, P., Turner, S. & Raymo, M.E., 2002. Geomagnetic excursions and paleointensities in the 0.9–2.15 Ma interval of the Matuyama Chron at ODP Site 983 and 984 (Iceland Basin), *J. geophys. Res.*, **107**(B6), doi:10.1029/2001JB000491.

Channell, J.E.T., Hodell, D.A., Xuan, C., Mazaud, A. & Stoner, J.S., 2008. Age calibrated relative paleointensity for the last 1.5 Myr at IODP Site U1308 (North Atlantic), *Earth planet. Sci. Lett.*, **274,** 59–71.

Chauvin, A., Roperch, P. & Duncan, R.A., 1990. Records of geomagnetic reversals from volcanic islands of French Polynesia 2. Paleomagnetic study of a flow sequence (1.2–0.6 Ma) from the island of Tahiti and discussion of reversal models, *J. geophys. Res.*, **95,** 2727–2752.

Chevallier, R. & Pierre, J., 1932. Propriétés magnétiques des roches volcaniques, *Ann. Phys.*, **18,** 383–477.

Clement, B.M., 1992. Evidence for dipolar fields during the Cobb Mountain geomagnetic polarity reversals, *Nature,* **358,** 405–407.

Clement, B.M., 2000. Comment on the Lau Basin Cobb Mountain records by Abrahamsen and Sager, *Phys. Earth planet. Inter,* **119,** 173–184.

Clement, B.M. & Martinson, D.G., 1992. A quantitative comparison of two paleomagnetic records of the Cobb Mountain Subchron zone from North Atlantic deep-sea sediments, *J. geophys. Res.*, **94,** 1735–1752.

Clouard, V., Bonneville, A. & Gillot, P.Y., 2001. A giant landslide on the southern flank of Tahiti Island, French Polynesia, *Geophys. Res. Lett.*, **28,** 11, doi:10.1029/2000GL012604.

Curewitz, D. & Karson, J.A., 1998. Geological consequences of dike intrusion at mid-ocean ridge spreading centers, in *Faulting and Magmatism at Mid-Ocean Ridges*, Geophysical Monograph 106, pp. 117–136, eds Buck, W.R., Delaney, P.T., Karson, J.A. & Lagabrielle, Y., American Geophysical Union, Washington, D.C.

Day, R., Fuller, M. & Schmidt, V.A., 1977. Hysteresis properties of titanomagnetites: grain size and compositional dependence, *Phys. Earth planet. Inter.*, **13,** 260–267.

Day, S.J., Heleno da Silva S.I.N. & Fonseca, J.F.B.D., 1999. A past giant lateral colapse and presente-day flank instability of Fogo, Cape Verde Islands, *J. Volc. Geotherm. Res.*, **94,** 191–218.

Delcamp, A., Petronis, M.S., Troll, V.R., Carracedo, J.C., van Wyk de Vries, B. & Pérez-Torrado, F.J., 2010. Vertical axis rotation of the upper portions of the north-east rift of Tenerife Island inferred from paleomagnetic data, *Tectonophysics*, **492,** 40–59.

DeMets, C., Gordon, R.G., Argus, D.F. & Stein, S., 1994. Effect of recent revisions to the geomagnetic reversal time scale on estimates of current plate motions. *Geophys. Res. Lett.*, **21,** 2191–2194.

Dias, N.A., Matias, L., Lourenço, N., Madeira, J., Carrilho, F. & Gaspar, J.L., 2007. Crustal seismic velocity structure near Faial and Pico Islands (AZORES), from local earthquake tomography, *Tectonophysics*, **445,** 301–317.

Dunlop, D.J., 2002. Theory and application of the Day plot (Mrs/Ms versus Hcr/Hc) 1: theoretical curves and tests using titanomagnetite data, *J. geophys. Res.*, **107,** 2056, doi:10.1029/2001JB000486.

Dunlop, D.J. & Özdemir, Ö., 1997. *Rock Magnetism: Fundamentals and Frontiers*, Cambridge Univ. Press, Cambridge, 573 pp.

Elsworth, D. & Voight, B., 1992. Theory of dike intrusion in a saturated porous solid, *J. geophys. Res.*, **97,** 9105–9117.

Féraud, G., Kaneoka, I. & Allègre, C.J., 1980. K/Ar ages and stress pattern in the Azores: geodynamic implications, *Earth planet. Sci. Lett.*, **46,** 275–286.

Fisher, R.A., 1953. Dispersion on a sphere, *Proc. R. Soc. London, A*, **217,** 98–102.

Foster, J.H. & Opdyke, N., 1970. Upper Miocene to recent magnetic straigraphy in deep-sea sediments, *J. geophys. Res.*, **75,** 4465–4473.

Gaspar, J.L., Queiroz, G., Pacheco, J.M., Ferreira, T., Wallenstein, N., Almeida, M.H. & Coutinho, R., 2003. Basaltic lava balloons produced during the 1998–2001 Serreta Submarine Ridge eruption (Azores), in *Subaqueous Explosive Volcanism*, Geophysical Monograph 140, pp. 205–212, eds White, J., Clague, D. & Smellie, J., American Geophysical Union, Washington, D.C.

Gente, P., Dyment, J., Maia, M. & Goslin, L., 2003. Interaction between the Mid-Atlantic Ridge and the Azores hot spot during the last 85 Myr: emplacement and rifting of the hot spot-derived plateaus, *Geochem. Geophys. Geosyst.*, **4,** 8514, doi:10.1029/2003GC000527.

Gillot, P.Y., Lefèvre, J.C. & Nativel, P.E., 1994. Model for the structural evolution of the volcanoes of Réunion Island, *Earth planet. Sci. Lett.*, **122,** 291–302.

Gillot, P.Y., Hildenbrand, A., Lefèvre, J.C. & Albore-Livadie, C., 2006. The K/Ar dating method: principle, analytical techniques and application to Holocene volcanic eruptions in southern Italy, *Acta Vulcanol.*, **18,** 55–66.

Hext, G., 1963. The estimation of second-order tensor, with related tests and designs, *Biometrika*, **50,** 353–357.

Hildenbrand, A., Gillot, P.Y., Soler, V. & Lahitte, P., 2003. Evidence for a persistent uplifting of La Palma (Canary Islands), inferred from morphological and radiometric data, *Earth planet. Sci. Lett.*, **210,** 277–289.

Hildenbrand, A., Gillot, P.Y. & Le Roy, I., 2004. Volcano-tectonic and geochemical evolution of an oceanic intra-plate volcano: Tahiti-Nui (French Polynesia), *Earth planet. Sci. Lett.*, **217,** 349–365.

Hildenbrand, A., Gillot, P.Y. & Bonneville, A., 2006. Off-shore evidence for a huge landslide of the northern flank of Tahiti-Nui (French Polynesia), *Geochem. Geophys. Geosyst.*, **7,** 1–12.

Hildenbrand A., Madureira P., Marques F.O., Cruz I., Henry B. & Silva, P.F., 2008. Volcanic evolution of S. Jorge Island, Azores (Central-North Atlantic): multi-stage development of a sub-aerial volcanic ridge over the last 1.4 Myr, *Earth planet. Sci. Lett.*, **273,** 289–298, doi:10.1016/j.epsl.2008.06.041.

Horng, C.-S., Lee, M.-Y., Palike, H., Wei, K.-Y., Liang, W.-T., Iizuka, Y. & Torii, M., 2002. Astronomically calibrated ages for geomagnetic reversals within the Matuyama chron, *Earth Planets Space*, **54,** 679–690.

Hsu, V., Merrill, D.L. & Shibuya, H., 1990. Paleomagnetic transition records of the Cobb Mountain event from sediment of the Celebes and Sulu Seas, *Geophys. Res. Lett.*, **17,** 2069–2072.

Jackson, M.J., Banerjee, S.K., Marvin, J.A., Lu, R. & Gruber, W., 1991. Detrital remanence, inclination errors, and anhysteretic remanence anisotropy: quantitative model and experimental results, *Geophys. J. Int.*, **104,** 95–103.

Jackson, A., Jonkers, A.R.T. & Walker, M.R., 2000. Four centuries of geomagnetic secular variation from historical records, *Phil. Trans. R. Soc., A*, **358,** 957–990.

Jelinek, V., 1978. Statistical processing of magnetic susceptibility measured in groups of specimens, *Stud. Geophys. Geod.*, **22,** 50–62.

Jelinek, V., 1981. Characterization of the magnetic fabric of rocks, *Tectonophysics*, **79,** 63–67.

Johnson, C.L. & Constable, C.G., 1995. The time averaged geomagnetic field as recorded by lava flows over the past 5 Myr, *Geophys. J. Int.*, **122,** 489–519.

Johnson, C.L. & Constable, C.G., 1997. The time averaged geomagnetic field: global and regional biases for 0–5 Ma, *Geophys. J. Int.*, **131,** 643–666.

Johnson, C.L., Wijbrans, J.R., Constable, C.G., Gee, J., Staudigel, H., Tauxe, L., Forjaz, V.-H. & Salgueiro, M., 1998. 40Ar/39Ar ages and paleomagnetism of São Miguel lavas, Azores, *Earth planet. Sci. Lett.*, **160,** 637–649.

Johnson, C.L. *et al.*, 2008. Recent investigations of the 0–5Ma geomagnetic field recorded by lava flows, *Geochem. Geophys. Geosyst.*, **9,** Q04032, doi:10.1029/2007GC001696.

Kent, D.V. & Smethurst, M.A., 1998. Shallow bias of paleomagnetic inclinations in the Paleozoic and Precambrian, *Earth planet. Sci. Lett.*, **160,** 391–402.

Kirschvink, J.L., 1980. The least squares line and plane and the analysis of paleomagnetic data, *Geophys. J. R. astr. Soc.*, **62,** 699–718.

Korte, M. & Constable, C.G., 2005. Continuous geomagnetic models for the past 7 millennia: 2. CALS7K, *Geochem. Geophys. Geosyst.*, **6,** Q02H16, doi:10.1029/2004GC000801.

Korte, M., Donadini, F. & Constable, C.G., 2009. Geomagnetic field for 0–3 ka: 2. A new series of time-varying global models, *Geochem. Geophys. Geosyst.*, **10,** Q06008, doi:10.1029/2008GC002297.

Kruiver, P.P., Dekkers, M.J. & Heslop, D., 2001. Quantification of magnetic coercivity components by the analysis of acquisition curves of isothermal remanent magnetization, *Earth planet. Sci. Lett.*, **189,** 269–276.

Lattard, D., Engelmann, R., Kontny, A. & Sauerzapf, U., 2006. Curie temperatures of synthetic titanomagnetites in the Fe-Ti-O system: effects of composition, crystal chemistry, and thermomagnetic methods, *J. geophys. Res.*, **111,** B12S28, doi:10.1029/2006JB004591.

Le Corvec, N. & Walter, T.R., 2009. Volcano spreading and fault interaction influenced by rift zone intrusions: insights from analogue experiments analyzed with digital image correlation technique, *J. Volc. Geotherm. Res.*, **183,** 170–182.

Lourenço, N., 2007. Tectono-magmatic processes in the Azores triple junction, *PhD thesis*, University of Algarve, Portugal.

Lourenço, N., Miranda, J.M., Luis, J.F., Ribeiro, A., Victor, L.A.M., Madeira, J. & Needham, H.D., 1998. Morpho-tectonic analysis of the Azores Volcanic Plateau from a new bathymetric compilation of the area, *Mar. Geophys. Res.*, **20,** 141–156.

Luis, J.F., 2007. Mirone: a multi-purpose tool for exploring grid data, *Comput. Geosci.*, **33**, 31–41.

Luis, J.F. & Miranda, J.M., 2008. Reevaluation of magnetic chrons in the North Atlantic between 35°N and 47°N: implications for the formation of the Azores triple junction and associated plateau, *J. geophys Res.*, **113,** B10105, doi:10.1029/2007JB005573.

Luis, J.F., Miranda, J.M., Galdeano, A., Patriat, P., Rossignol, J.C. & Mendes Victor, L.A., 1994. The Azores triple junction evolution since 10 Ma from an aeromagnetic survey of the Mid-Atlantic Ridge, *Earth planet. Sci. Lett.*, **125,** 439–459.

Luis, J.F., Lourenço, N., Miranda, J.M., Gaspar, J.L. & Queiroz, G., 1999. A submarine eruption West of Terceira Island (Azores Archipelago), *Interridge News*, **8,** 13–14.

Lyakhovsky, V., Ben-Zion, Y. & Agnon, A., 1997. Distributed damage, faulting, and friction, *J. geophys. Res.*, **102,** 635–27, 649, doi:10.1029/97JB01896.

Machado, F., Parsons, W., Richards, A. & Mulford, J.W., 1962. Capelinhos eruption of Fayal Volcano, Azores, 1957–1958, *J. geophys. Res.*, **67,** 3519–3529.

Madeira, J., 1998. Estudos de neotectónica nas ilhas do Faial, Pico e S. Jorge: Uma contribuição para o conhecimento geodinâmico da junção tripla dos Açores, *PhD thesis*, Univ. of Lisboa, 481pp.

Madeira, J. & Ribeiro, A., 1990. Geodynamic models for the Azores triple junction: a contribution for tectonics, *Tectonophysics*, **184,** 405–415.

Madureira, P., Moreira, M., Mata, J. & Allègre, C.J., 2005. Primitive neon isotopes in Terceira Island (Azores archipelago), *Earth planet. Sci. Lett.*, **233,** 429–440.

Madureira, P., Mata, J., Mattielli, N., Queiroz, G. & Silva, P., 2011. Mantle source heterogeneity, magma generation and magmatic evolution at Terceira Island (Azores archipelago): constraints from elemental and isotopic (Sr, Nd, Hf, and Pb) data. *Lithos*, **126,** 402–418.

Mankinen, E.A. & Gromme, C.S., 1982. Paleomagnetic data from the Coso Range, California and current status of the Cobb Mountain geomagnetic polarity event, *Geophys. Res. Lett.*, **9,** 1279–1282.

Mankinen, E.A., Donnelly, J.M. & Grommé, C.S., 1978. Geomagnetic polarity event recorded at 1.1 m.y. B.P. on Cobb Mountain, Clear Lake volcanic field, California, *Geology*, **8,** 653–656.

Mankinen, E.A., Donnelly-Nolan, J.M., Gromme, C.S. & Hearn, B.C., Jr, 1981. Paleomagnetism of the Clear Lake Volcanics and new limits on the age of the Jaramillo normal polarity event, *Research in the Geysers-Clear Lake Geothermal Area, Northern California*, US Geol. Surv. Prof. Paper 1141, pp. 67–82, eds McLaughlin, R.J. & Donnelly-Nolan, J.M., USGS, Reston, VA.

Mériaux, C. & Lister, J.R., 2002. Calculation of dike trajectories from volcanic centers, *J. geophys. Res.*, **107,** 2077, doi:10.1029/2001JB000436.

Mériaux, C., Lister, J.R., Lyakhovsky, V. & Agnon, A. 1999. Dyke propagation with distributed damage of the host rock, *J. geophys. Res.*, **165,** 177–185.

McElhinny, M.W. & McFadden, P.L., 1997. Palaeosecular variation over the past 5 Myr based on a new generalized database, *Geophys. J. Int.*, **131,** 240–252.

McFadden, P.L. & Lowes, F.J., 1981. The discrimination of mean directions drawn from Fisher distributions, *Geophys. J. R. astr. Soc.*, **67,** 19–33.

McFadden, P.L. & McElhinny, M.W., 1990. Classification of the reversal test in palaeomagnetism, *Geophys. J. Int.*, **103,** 725–729.

McFadden, P.L., Merrill, R.T. & McElhinny, M.W., 1988. Dipole quadrupole family modeling of paleosecular variation, *J. geophys. Res.*, **93,** 11 583–11 588.

Merle, O. & Lénat, J.-F., 2003. Hybrid collapse mechanism at Piton de la Fournaise volcano, Reunion Island, Indian Ocean, *J. geophys. Res.*, **108,** 2166, doi:10.1029/2002JB002014.

Miranda, M., Luis, J.F., Abreu, I., Victor, L.A., Galdeano, A. & Rossignol, J.C., 1991. Tectonic framework of the Azores triple junction, *Geophys. Res. Lett.*, **18,** 1421–1424.

Miranda, J.M. *et al*., 1998. Tectonic setting of the Azores Plateau deduced from a OBS survey, *Mar. Geophys. Res.*, **20,** 171–182.

Miranda, J.M., Silva, P., Lourenço, N., Henry, B., Costa, R. & SALDANHA TEAM, 2002. Study of the Saldanha massif (MAR, 36°34'N): constrains from rock magnetic and geophysical data, *Mar. Geophys. Res.*, **23,** 299–318.

Moore, J.G., Clague, D.A., Holcomb, R.T., Lipman, P.W., Normark, W.R. & Torresan, M.E., 1989. Prodigious submarine landslides on the Hawaiian ridge, *J. geophys. Res.*, **94,** 17 465–17 484.

Morgan, J.K. & Clague, D.A., 2003. Volcanic spreading on Mauna Loa volcano, Hawaii: evidence from accretion, alteration, and exhumation of volcaniclastic sediments, *Geology*, **31,** 411–414.

O'Reilly, W. (ed.), 1984. *Rock and Mineral Magnetism*, CRC Press, Boca Raton, FL, 220pp.

Owen, S., Segall, P., Lisowski, M., Miklius, A., Denlinger, R. & Sako, M., 2000. Rapid deformation of Kilauea Volcano: Positioning System measurements between 1990 and 1996, *J. geophys. Res.*, **105,** B8, doi:10.1029/2000JB900109.

Özdemir, Ö., 1987. Inversion of titanomaghemites, *Phys. Earth planet. Inter.*, **46,** 184–196.

Petrovský, E. & Kapička, A. 2006. On determination of the Curie point from thermomagnetic curves, *J. geophys. Res.*, **111,** B12S27, doi:10.1029/2006JB004507.

Quidelleur, X. & Valet, J.P., 1996. Geomagnetic changes across the last reversal recorded in lava flows from La Palma, Canary Islands, *J. geophys. Res.*, **101,** 13 755–13 773.

Quidelleur, X. Valet, J.P., Courtillot, V. & Hulot, G., 1994. Long-term geometry of the geomagnetic field for the last five million years: an updated secular variation database, *Geophys. Res. Lett.*, **21**(15), 1639–1642.

Quidelleur, X., Carlut, J., Soler, V., Valet, J.-P. & Gillot, P.-Y., 2003. The age and duration of the Matuyama-Brunhes transition from new K/Ar data from La Palma (Canary Islands) and revisited $^{40}Ar/^{39}Ar$ ages, *Earth planet. Sci. Lett.*, **208,** 149–163.

Quidelleur, X., Hildenbrand, A. & Samper, A., 2008. Causal link between Quaternary paleoclimatic changes and volcanic islands evolution, *Geophys. Res. Lett.*, **35,** L02303, doi:10.1029/2007GL031849.

Readman, P.W. & O'Reilly, W., 1972. Magnetic properties of oxidized (cation-deficient) titanomagnetites, $(Fe, Ti, \square)_3O_4$, *J. Geomagn. Geoelectr.*, **24,** 69–90.

Renne, P.R., Swisher, C.C., Deino, A.L., Karner, D.B., Owens, T.L. & DePaolo, D.J., 1998. Intercalibration of standards, absolute ages and uncertainties in 40Ar/39Ar dating, *Chem. Geol.*, **145,** 117–152.

Reisinger, J., Edel, J.B. & Mauritsch, H.J., 1994. Late Carboniferous—Late Permian paleomagnetic overprinting of Carboniferous granitoids in southern Bohemian Massif (Austria), *Phys. Earth planet. Inter.*, **85,** 53–65.

Riley, C.M., Diehl, J.F. Kirschvink, J.L. & Ripperdan, R.L., 1999. Paleomagnetic constraints on fault motion in the Hilina Fault System, south flank of Kilauea Volcano, Hawaii, *J. Volc. Geotherm. Res.*, **94,** 233–249.

Robertson, D.J. & France, D.E., 1994. Discrimination of remanence-carrying minerals in mixtures, using isothermal remanent magnetisation acquisition curves, *Phys. Earth planet. Inter.*, **82,** 223–234.

Rubin, A.M., 1995. Propagation of magma-field cracks, *Ann. Rev. Earth planet. Sci.*, **23,** 287–336.

Rubin, A.M. & Pollard, D.D., 1988. Origins of blade-like dikes in volcanic rifts zones, in *Volcanism in Hawaii*, U.S. Geol. Surv. Prof. Paper 1350, pp. 1449–1470, eds Decker, R.W., Wright, T.L. & Sauffer, P.H., USGS, Reston, VA.

Searle, R., 1980. Tectonic pattern of the Azores spreading centre and triple junction, *Earth planet. Sci. Lett.*, **51,** 415–434.

Shackleton, N.J., Berger, A. & Peltier, W.R., 1990. An alternative astronomical calibration of the lower Pleistocene timescale based on ODP site 677, *Trans. R. Soc. Edinburgh, Earth Sci.*, **81,** 251–261.

Silva, P.F., Henry, B., Marques, F.O., Madureira, P. & Miranda, J.M., 2006a. Paleomagnetic study of the Great Foum Zguid dyke (Southern Morocco): a positive contact test related to metasomatic processes, *Geophys. Res. Lett.*, **33,** L21301, doi:10.1029/2006GL027498.

Silva, P.F., Henry, B., Marques, F.O., Mateus, A., Madureira, P., Lourenço, N. & Miranda, J.M., 2006b. Variation of magnetic properties in sedimentary rocks hosting the Foum Zguid dyke (Southern Morocco): combined effects of re-crystallization and Fe-metasomatism, *Earth planet. Sci. Lett.*, **241,** 978–992.

Silva P.F. *et al*., 2008. Magma flow, exsolution processes and rock metasomatism in the Great Messejana-Plasencia dyke (Iberian Peninsula), *Geophys. J. Int.*, **175,** 806–824, doi:10.1111/j.1365-246X.2008.03920.x.

Silva, P.F., Marques, F.O., Henry, B., Madureira, P., Hirt, A.M., Font, E. & Lourenço, N., 2010. Thick dyke emplacement and internal flow: a structural and magnetic fabric study of the deep-seated dolerite dyke of Foum Zguid (southern Morocco), *J. geophys Res.*, **115,** B12108, doi:10.1029/2010JB007638.

Singer, B.S., Hoffman, K.A., Chauvin, A. & Coe, R.S., 1999. Dating transitionally magnetized lavas of the late Matuyama Chron: toward a new 40Ar/39Ar timescale of reversals and events, *J. geophys. Res.*, **104,** 679–693.

Steiger, R.H. & Jäger, E., 1977. Subcommission on 927 geochronology: convention on the use of decay constants in geo and cosmochronology, *Earth planet. Sci. Lett.*, **36,** 359–362.

Storetvedt, K.M., Mongstad Vage, H., Aase, S. & Lovlie, R., 1979. Palaeomagnetism and the early magmatic history of Fuerteventura (Canary Islands), *J. Geophys.*, **46,** 319–334.

Sueishi, T., Sato, N. & Kobayashi, K., 1979. Short geomagnetic episode in the Matuyama Epoch, *Phys. Earth planet. Inter.,* **19,** 1–11.

Tauxe, L., 2005. Inclination shallowing and the geocentric axial dipole hypothesis. *Earth planet. Sci. Lett.,* **233,** 247–261.

Tauxe, L., Mullender, T.A.T. & Pick, T., 1996. Pot-bellies, wasp-waists and superparamagnetism in magnetic hysteresis, *J. geophys. Res.,* **101,** 571–583.

Turrin, B.D., Donnelly-Nolan, J.M., Carter, B. & Hearn, J., 1994. $^{40}Ar/^{39}Ar$ ages from the rhyolite of Alder Creek, California: age of the Cobb Mountain normal polarity subchron revisited, *Geology,* **22,** 251–254.

Van der Voo, R. & Torsvik, T.H., 2001. Evidence for late Paleozoic and Mesozoic non-dipole fields provides an explanation for the Pangea reconstruction problems, *Earth planet. Sci. Lett.,* **187,** 71–81.

Vandamme, D., 1994. A new method to determine paleosecular variation, *Phys. Earth planet. Inter.,* **85,** 131–142.

Vogt, P.R. & Jung, W.Y., 2004. The Terceira rift as hyper-slow, hotspot-dominated oblique spreading axis: a comparison with other slow-spreading plate boundaries, *Earth planet. Sci. Lett.,* **218,** 77–90.

Walker, G.P.L., 1988. Three Hawaiian calderas: an origin through loading by shallow intrusions?, *J. geophys. Res.,* **93,** 14 773–14 784.

Watkins, N.D., 1968. Short period geomagnetic events in deep-sea sedimentary cores, *Earth planet. Sci. Lett.,* **4,** 342–349.

Watkins, N.D., 1973. Palaeomagnetism of the Canary Islands and Madeira, *Geophys. J. R. astr. Soc.,* **32,** 249–267.

Wilson, R.I., Haggerty, S.E. & Watkins, N.D., 1968. Variation of palaeomagnetic stability and other parameters in a vertical traverse of a single Icelandic lava, *Geophys. J. R. astr. Soc.,* **16,** 79–96.

Yukutake, T., 1971. Spherical harmonic analysis of the Earth's magnetic field for the 17th and 18th centuries, *J. Geomagn.Geoelectr.,* **23,** 11–23.